primer set: 5′-gtgagtagctcgctccgc-3′ and 5′-ctgagggggca-gagggtc-3′. The amplified DNA was cloned into pGL3 Promoter vector (Promega Corporation) to construct the Dll4-Int3-Luc reporter plasmid. To generate the Dll4-Int3mut-Luc reporter plasmid, the RBP-J binding site was mutated using the QuikChange Site-directed Mutagenesis kit (Stratagene) with the Dll4-Int3-Luc plasmid as a template. To construct the p3xFLAG-NICD plasmid encoding FLAG-tagged NICD, a DNA fragment encoding the Notch1 intracellular domain was excised from the pcDNA-FLAG-Notch1-ICD vector, a gift from M. Kurabayashi (Gunma University), and subcloned into p3xFLAG-CMV10 vector (Sigma). A cDNA encoding human Foxc2 was amplified by PCR using human heart cDNAs as a template, and cloned into pERed-NLS vector, a gift from M. Matsuda (40), namely pERed-NLS-Foxc2 plasmid. A 3.7-kb fragment of the mouse Dll4 promoter (−3631/+76) cloned in the pGL3 Basic vector (Promega Corporation) has already been reported (41). An expression plasmid encoding the constitutively active form of β-catenin (CA-βCat) in which Ser^{37} is replaced with Ala, was kindly provided by J. S. Gutkind (National Institute of Health). Other vectors are purchased as follows: pRL-SV40 and pRL-TK from Promega Corporation and TOPflash reporter plasmid from Millipore Corporation. Recombinant adenovirus vectors encoding LacZ and the constitutively active form of AKT (CA-AKT) were kindly provided by M. Matsuda (Kyoto University) and Y. Fujio (Osaka University), respectively.

Real Time Reverse Transcription-PCR—Endothelial cells placed on collagen-coated plates under either sparse or confluent culture conditions were starved in medium 199 containing 1% BSA for 12 h, and stimulated with either 400 ng/ml of COMP-Ang1 or 10 μM SB216763 as described in the figure legends. After stimulation, total RNA was purified using TRIzol (Invitrogen). Quantitative real time reverse transcription (RT)-PCR was carried out using the QuantiFast SYBR Green RT-PCR kit (Qiagen) as described (12). For each reaction, 100 ng of total RNA was transcribed for 10 min at 50 °C, followed by a denaturing step at 95 °C for 5 min and 40 cycles of 10 s at 95 °C and 30 s at 60 °C. Fluorescence data were collected and analyzed using Mastercycler ep realplex (Eppendorf). The primers used for amplification were as follows: human *Dll4*, 5′-tccaactgc-ccttcaatttcac-3′ and 5′-ctggatggcgatcttgctga-3′; for glyceraldehyde-3-phosphate dehydrogenase (*GAPDH*), 5′-atggg-gaaggtgaaggtcg-3′ and 5′-ggggtcattgatggcaacaata-3′. For normalization, expression of human *GAPDH* was determined in parallel as an endogenous control.

Immunoprecipitation and Western Blot Analysis—Confluent and sparse HUVECs plated on a collagen-coated dish were starved in medium 199 containing 1% BSA for 12 h, and stimulated as described in the figure legends. After stimulation, the cells were lysed in ice-cold lysis buffer containing 50 mM Tris-HCl, pH 7.5, 150 mM NaCl, 1% Triton X-100, 0.5% sodium deoxycholate, 0.1% SDS, 20 mM sodium fluoride, 1 mM sodium vanadate, and 1× protease inhibitor mixture (Roche Applied Science), and centrifuged at 15,000 × *g* for 20 min at 4 °C. The supernatant was used as precleared cell lysate. To detect the Dll4 protein expression and the NICD production, the cell lysates were subjected to SDS-PAGE and Western blot analysis with anti-Dll4 and anti-NICD antibodies. To evaluate phosphorylation of AKT and GSK3β, aliquots of cell lysate were subjected to Western blot analysis with anti-phospho-AKT and anti-phospho-GSK3β antibodies, respectively. The total contents of AKT and GSK3β in each cell lysate were also assayed in a parallel run using corresponding antibodies. To detect interaction between NICD and β-catenin, NICD was immunoprecipitated with anti-NICD antibody from the precleared lysates. Immunoprecipitated NICD and aliquots of cell lysate were subjected to SDS-PAGE and Western blot analysis with anti-β-catenin and anti-NICD antibodies, respectively.

Luciferase Reporter Assay—Luciferase reporter assay was performed as described previously (42). Briefly, HUVECs plated on a collagen-coated dish were transfected with different expression vectors, together with reporter plasmids as described in the figure legends. The total amount of plasmid DNA was adjusted with empty vector. The cells were harvested, and re-plated on the collagen-coated 24-well plate in confluent culture conditions. Luciferase activity was assayed 48 h after the transfection. To examine the effect of COMP-Ang1, the cells were starved and stimulated as described in the figure legends. The cells were lysed using passive lysis buffer (Promega Corporation), and luciferase activities in cell extract were determined using a dual luciferase assay system (Promega Corporation).

Chromatin Immunoprecipitation Assay—Chromatin immunoprecipitation (ChIP) assay was performed using the EZ ChIP™ kit (Millipore Corporation) according to the manufacturer's instructions. Confluent HUVECs plated on collagen-coated dishes were starved in medium 199 containing 1% BSA for 12 h, and stimulated with 400 ng/ml of COMP-Ang1 for 30 min. After stimulation, genomic DNA and protein were cross-linked by addition of formaldehyde (1% final concentration) directly to culture medium, and incubated for 10 min at room temperature (RT). The cells were then harvested, lysed, and sonicated to generate 0.3–1.0-kb DNA fragments. After centrifugation, the cleared supernatant was incubated with anti-RBP-J, anti-NICD, anti-β-catenin, and control antibodies for immunoprecipitation. Co-immunoprecipitated and input DNA were used as a template for PCR amplification. PCR amplifications were carried out using the primers specific for intron 3 of the human *Dll4* gene (5′-gacgcttagcttggcctg-gagctg-3′ and 5′-tgtaaaatacaggaaggggcccgtcag-3′). PCR sensitivity was evaluated with serial dilutions of input DNA collected after sonication. Amplified DNA was separated on 2% agarose gels and visualized with ethidium bromide.

Endothelial Cell Tube Formation Assay—Endothelial cell tube formation assay was performed according to the method of Davis and co-workers (43). HUVECs were suspended in 2.5 mg/ml of collagen type I matrices (Nitta Gelatin) at a density of 2×10^6 cells/ml, and incubated at 37 °C for 48 h in medium 199 containing reduced serum supplement, bFGF at 40 ng/ml, and ascorbic acid at 50 μg/ml. During the incubation, the cells were stimulated with or without COMP-Ang1 in the presence or absence of 20 μM DAPT. The cultures were fixed in PBS containing 2% paraformaldehyde for 2 h at RT, and blocked with PBS containing 1% BSA for 12 h at 4 °C. To detect extracellular deposition of collagen type IV, the cultures were stained with anti-collagen type IV antibody for 12 h at 4 °C, and visualized

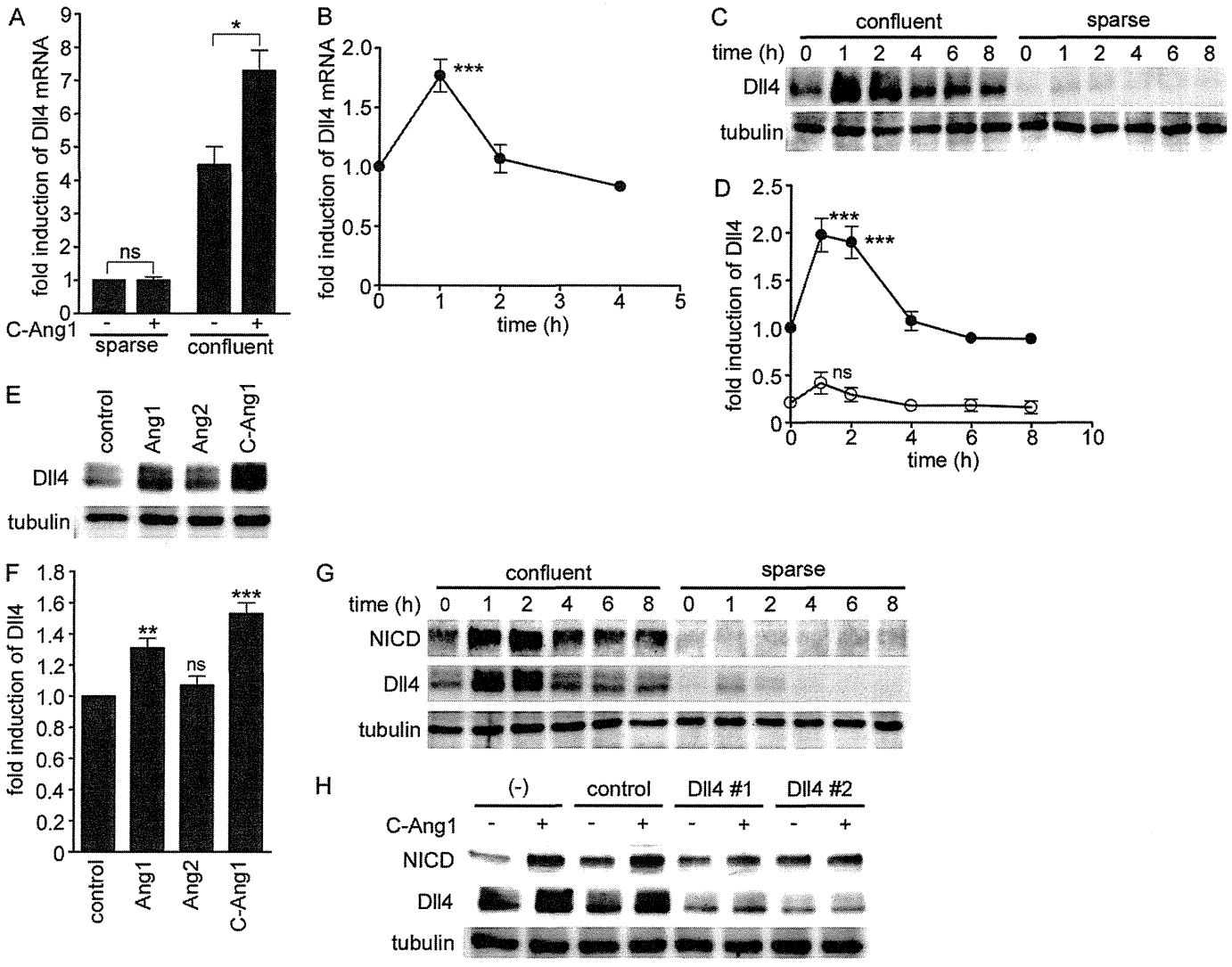

FIGURE 1. **Ang1 induces Dll4 expression leading to activation of Notch signaling in confluent endothelial cells.** *A*, sparse and confluent HUVECs were starved in medium 199 containing 1% BSA for 12 h, and stimulated with vehicle (−) or COMP-Ang1 at 400 ng/ml (*C-Ang1*) for 1 h. (COMP-Ang1 was used at the concentration of 400 ng/ml throughout the following experiments.) After stimulation, total RNA was extracted and subjected to real time RT-PCR analysis to determine the expression of Dll4 mRNA as described under "Experimental Procedures." *Bar graphs* show relative mRNA levels of Dll4 mRNA normalized to that of GAPDH. Data are expressed as fold-induction relative to that in the vehicle-treated sparse cells, and shown as mean ± S.D. of three independent experiments. *B*, confluent HUVECs starved for 12 h were stimulated with COMP-Ang1 for the periods indicated at the *bottom* (*h*). Dll4 mRNA levels were analyzed by real time RT-PCR as described in *A*. Values are expressed as fold-induction relative to that in the unstimulated cells, and shown as mean ± S.D. of five independent experiments. *C*, confluent and sparse HUVECs were starved in medium 199 containing 1% BSA for 12 h, and stimulated with COMP-Ang1 for the periods indicated at the *top* (*h*). Cell lysates were subjected to Western blot analysis with anti-Dll4 (Dll4) and anti-tubulin (tubulin) antibodies. *D*, the relative expression of Dll4 observed in *C* are quantified by normalizing the expression of Dll4 by that of tubulin. Values are expressed as fold-induction relative to that observed in the confluent unstimulated cells, and shown as mean ± S.D. of three independent experiments. *E*, confluent HUVECs starved for 12 h were stimulated with vehicle (*control*), 600 ng/ml of Ang1 (*Ang1*), 600 ng/ml of Ang2 (*Ang2*) and COMP-Ang1 (*C-Ang1*) for 1 h. Cell lysates were subjected to Western blot analysis with anti-Dll4 (Dll4) and anti-tubulin (tubulin) antibodies. *F*, expression of Dll4 protein observed in *E* are quantified as described in *D*. Values are expressed as fold-induction relative to that observed in the control cells, and shown as mean ± S.D. of four independent experiments. *G*, confluent and sparse HUVECs were starved in medium 199 containing 1% BSA for 12 h, and stimulated with COMP-Ang1 for the periods indicated at the *top* (*h*). Cell lysates were subjected to Western blot analysis with anti-NICD (*NICD*), anti-Dll4 (*Dll4*), and anti-tubulin (*tubulin*) antibodies. *H*, confluent HUVECs transfected without (−) or with either control siRNA (*control*) or two independent siRNAs targeting Dll4 (*Dll4#1* and *Dll4#2*) were stimulated with COMP-Ang1 as described in *A*. Cell lysates were subjected to Western blot analysis with anti-NICD (*NICD*), anti-Dll4 (*Dll4*), and anti-tubulin (*tubulin*) antibodies. Significant differences between two groups (*A*) or from the control (*B*, *D*, and *F*) are indicated as: *, $p < 0.05$; **, $p < 0.01$; or ***, $p < 0.001$. *n.s.* indicates no significance between two groups or from the control.

with Alexa 488-labeled donkey anti-goat IgG. To visualize filamentous actin, the cultures were subsequently permeabilized with 0.1% Triton X-100 for 1 h at RT, and stained with rhodamine-phalloidin for 12 h at 4 °C. Fluorescence images of Alexa 488 and rhodamine were recorded with a FV1000 confocal microscope (Olympus Corporation) with a ×20 water immersion objective lens. To quantify the extracellular deposition of collagen type IV, fluorescence intensity of Alexa 488 within the areas of the rhodamine-marked tube structures was determined using FluoView software (Olympus Corporation). Data were expressed as average pixel intensity in the areas of tube structures.

Statistical Analysis—The values are expressed as mean ± S.D. Statistical significance was determined using one-way analysis of variance or unpaired *t* test. p values < 0.05 were considered statistically significant.

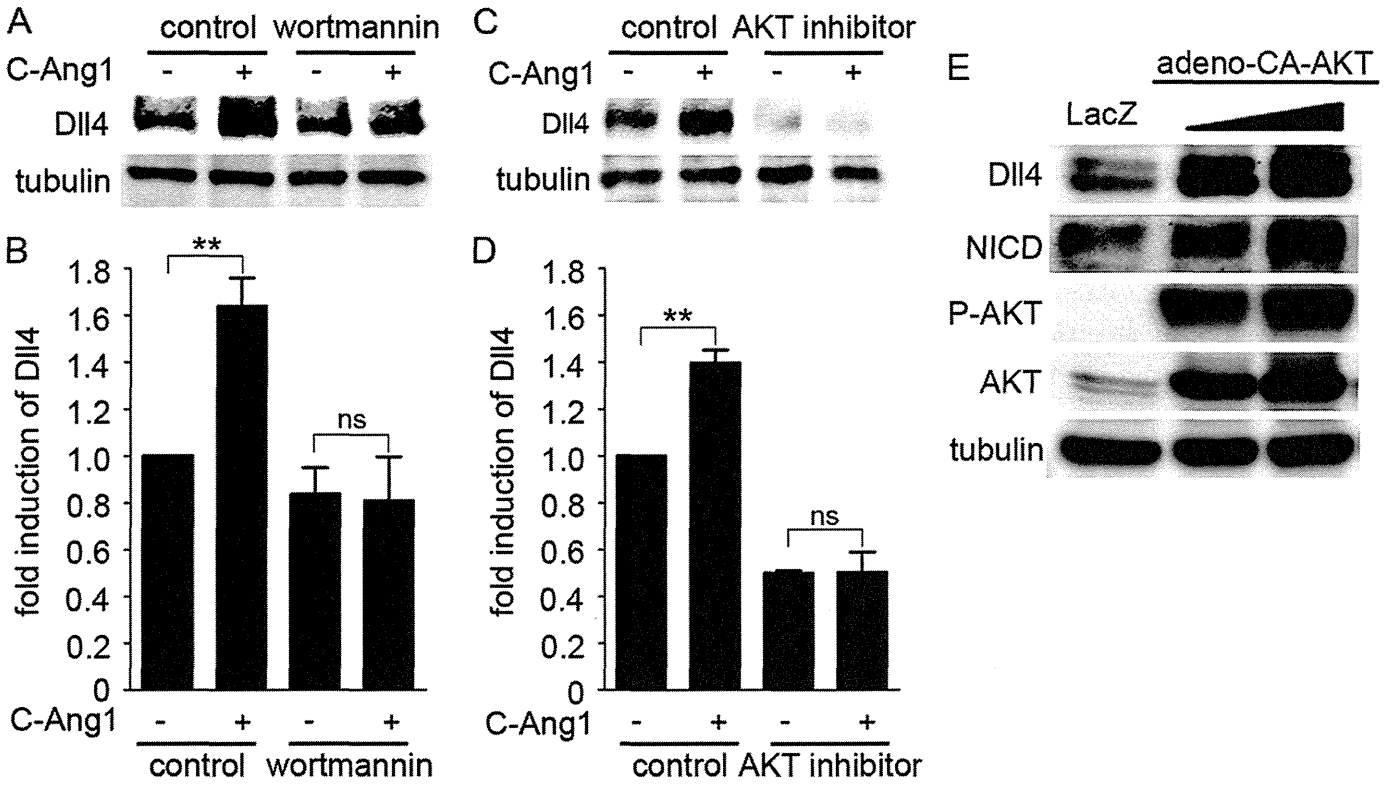

FIGURE 2. **Ang1 induces Dll4 expression through a PI3K/AKT pathway.** *A*, confluent HUVECs starved for 12 h were pretreated with vehicle (*control*) or 60 nM wortmannin for 30 min, and subsequently stimulated with vehicle (−) or COMP-Ang1 (+) for 1 h. Dll4 protein expression was examined by Western blot analysis as described in the legend of Fig. 1*C*. *B*, expression of Dll4 protein observed in *A* are quantified as described in legend of Fig. 1*D*. Values are expressed as fold-induction relative to that in the wortmannin-untreated cells stimulated with vehicle, and shown as mean ± S.D. of five independent experiments. *C*, confluent HUVECs starved for 12 h were pretreated with vehicle (control) or 8 μM AKT inhibitor for 10 min and subsequently stimulated with vehicle (−) or COMP-Ang1 (+) for 1 h. Dll4 protein expression was analyzed as described in *A*. *D*, expression of Dll4 protein observed in *C* are quantified as described in legend of Fig. 1*D*. Values are expressed as fold-induction relative to that in the AKT inhibitor-untreated cells stimulated with vehicle, and shown as mean ± S.D. of four independent experiments. *E*, confluent HUVECs were infected with adenoviruses encoding LacZ or with two different titers of adenoviruses encoding AKT-CA for 48 h. Cell lysates were subjected Western blot analysis with anti-Dll4 (*Dll4*), anti-NICD (*NICD*), anti-phospho-AKT (*P-AKT*), anti-AKT (*AKT*), and anti-tubulin (*tubulin*) antibodies. Significant differences between two groups (*B* and *D*) are indicated as: **, $p < 0.01$. *n.s.* indicates no significance between two groups.

RESULTS

Ang1 Induces Notch Signaling by Up-regulating Dll4 under Confluent, But Not Sparse Cultures of HUVECs—We previously found that Dll4 expression was up-regulated in confluent HUVECs stimulated with Ang1 by the microarray analyses (10). To first confirm whether Dll4 expression is increased by Ang1 in the HUVECs with cell-cell contacts, HUVECs were stimulated with COMP-Ang1, a potent Ang1 variant, under either confluent or sparse culture conditions. Before the stimulation, *Dll4* mRNA was ~4 times higher in confluent HUVECs than in the sparse cells, indicating that the basal Notch signal is present in the HUVECs with cell-cell contacts (Fig. 1*A*). COMP-Ang1 significantly increased *Dll4* mRNA in the confluent HUVECs, which peaked at 1 h after the stimulation and immediately declined to the basal level by 2 h (Fig. 1, *A* and *B*). Similarly, *DLL4* mRNA levels were increased by stimulation with COMP-Ang1 in human aortic endothelial cells and human dermal microvascular endothelial cells under confluent culture conditions (supplemental Fig. S1). However, in the sparse HUVECs, *DLL4* mRNA was not affected by the stimulation with COMP-Ang1 (Fig. 1*A*). Consistently, Dll4 in the confluent HUVECs was higher than that in the sparse cells, and was increased in response to COMP-Ang1 (Fig. 1, *C* and *D*). In contrast, COMP-Ang1 did not induce Dll4 in the sparse cells (Fig. 1, *C* and *D*). Dll4 was induced by native Ang1 as well as COMP-Ang1, but not by Ang2, an antagonist for Tie2 (Fig. 1, *E* and *F*). These results suggest that Dll4 up-regulation by Ang1 depends on the cell-cell contacts that allow activation of Notch signaling, and is dependent on the specific signal downstream of the *trans*-associated Tie2 by Ang1.

To further investigate whether Dll4 expression by *trans*-associated Tie2 leads to activation of Notch signaling, we examined the amount of NICD. COMP-Ang1 increased NICD in parallel with Dll4 up-regulation under confluent culture conditions, which peaked at 1–2 h after stimulation and declined to basal levels by 4 h, although NICD was not induced by COMP-Ang1 in the sparse cells (Fig. 1*G*). In addition, depletion of Dll4 by siRNA blocked increase in NICD by COMP-Ang1 (Fig. 1*H*). Collectively, these results indicate that Tie2 activation in the presence of cell-cell contacts results in activation of Notch signaling by up-regulating Dll4 expression.

A PI3K/AKT Pathway Is Involved in Ang1-induced Dll4 Expression—To understand the molecular mechanism underlying Dll4 expression by Ang1/Tie2 in confluent cells, we focused on the downstream signaling of Tie2 in the presence of cell-cell contacts. We previously demonstrated that the PI3K/

AKT signal is preferentially activated by *trans*-associated Tie2 (10). Thus, we next investigated involvement of the PI3K/AKT pathway in Ang1-induced Dll4 expression by using specific inhibitors for PI3K (wortmannin) and AKT (AKT inhibitor). Either inhibitor prevented not only COMP-Ang1-induced AKT activation but also COMP-Ang1-induced Dll4 expression (Fig. 2, *A–D*, and supplemental Fig. S2, *A* and *B*), indicating the requirement of the PI3K/AKT pathway for Ang1-induced Dll4 expression. We further tested whether activation of the PI3K/AKT pathway is sufficient to induce Dll4 expression by infecting HUVECs with adenovirus-encoding CA-AKT, an active mutant of AKT. Overexpression of CA-AKT led to the increase in both Dll4 and NICD (Fig. 2*E*). These findings indicate that Ang1 activates Notch signaling through the PI3K/AKT pathway-mediated Dll4 expression.

GSK3β Is a Downstream Target of AKT Responsible for Ang1-induced Dll4 Expression—Among the substrates of AKT, GSK3β is a well documented downstream target of the PI3K/AKT pathway that regulates various cellular functions (44). Thus, we investigated whether GSK3β acts downstream of the PI3K/AKT pathway to mediate Ang1-induced Dll4 expression. AKT phosphorylates GSK3β on Ser^9 to render it inactive (44). Therefore, we examined the effect of Ang1 on GSK3β phosphorylated at Ser^9 by using the anti-phospho-GSK3β antibody. COMP-Ang1 induced an increase in the phosphorylation of GSK3β, which peaked at 30 min after the stimulation (Fig. 3*A*). COMP-Ang1-induced GSK3β phosphorylation was inhibited by wortmannin (Fig. 3, *B* and *C*). Consistently, adenovirus-mediated overexpression of CA-AKT resulted in increased GSK3β phosphorylation in HUVECs (Fig. 3*D*). These results indicate that Ang1 inhibits GSK3β through phosphorylation by AKT. We further tested whether GSK3β inactivation is sufficient to induce Dll4 expression. Confluent but not sparse HUVECs treated with GSK3β inhibitors, LiCl and SB216763, exhibited up-regulation of Dll4 and an increase in NICD (Fig. 3, *E* and *F*, and supplemental Fig. S3). Collectively, these findings reveal that Ang1 induces Dll4 expression through AKT-mediated inactivation of GSK3β.

β-Catenin Is Required for Ang1-induced Dll4 Expression—β-Catenin is one of the major substrates of GSK3β, and undergoes proteasomal degradation through GSK3β-mediated phosphorylation (45). Recently, Corada *et al.* (46) have reported that the Wnt/β-catenin pathway up-regulates Dll4 transcription through the TCF-binding site located 706 bp upstream from the transcription start site of mouse *Dll4* gene. Considering these evidences, we hypothesized that stabilization of β-catenin through AKT-mediated inactivation of GSK3β is involved in Ang1-induced Dll4 expression. To address this possibility, HUVECs were transfected with a β-catenin-responsive luciferase reporter construct containing four native TCF binding sites (TOPflash). COMP-Ang1 significantly induced luciferase activity driven by TOPflash reporter (Fig. 4*A*), indicating the ability of Ang1 to induce β-catenin-dependent transcription. We further clarified the requirement of β-catenin in Ang1-induced Dll4 expression by transfecting HUVECs with two independent siRNAs targeting β-catenin. Depletion of β-catenin by siRNAs completely abolished COMP-Ang1-induced Dll4 expression (Fig. 4*B*). Similarly, Dll4 expression

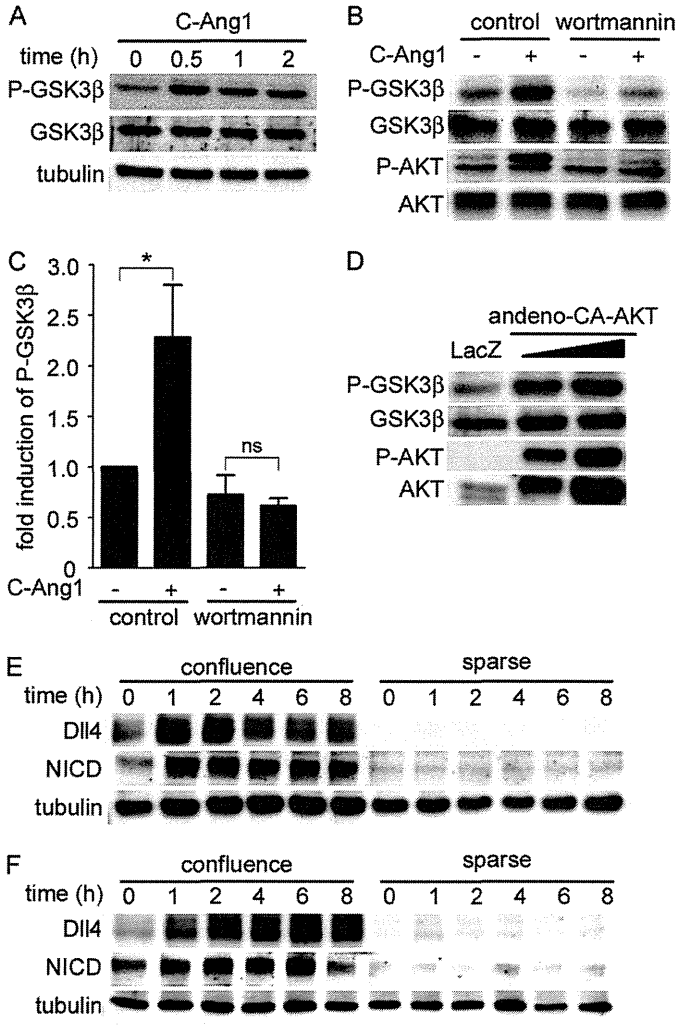

FIGURE 3. **Ang1 induces Dll4 expression through AKT-mediated inhibition of GSK3β.** *A*, confluent HUVECs starved for 12 h were stimulated with COMP-Ang1 for the periods indicated at the *top* (*h*). Cell lysates were subjected to Western blot analysis with anti-phospho-GSK3β (*P-GSK3β*), anti-GSK3β (*GSK3β*), and anti-tubulin (*tubulin*) antibodies. *B*, confluent HUVECs starved for 12 h were pretreated with vehicle (*control*) or 60 nM wortmannin for 30 min, and subsequently stimulated with vehicle (−) or COMP-Ang1 (+) for 30 min. Cell lysates were subjected to Western blot analysis with anti-phospho-GSK3β (*P-GSK3β*), anti-GSK3β (*GSK3β*), anti-phospho-AKT (*P-AKT*), and anti-AKT (*AKT*) antibodies. *C*, phosphorylated GSK3β levels observed in *B* are quantified by normalizing the expression of phosphorylated GSK3β by that of total GSK3β. Values are expressed as fold-induction relative to that in the wortmannin-untreated cells stimulated with vehicle, and shown as mean ± S.D. of three independent experiments. *D*, confluent HUVECs were infected with adenoviruses encoding either LacZ or CA-AKT. Cell lysates were subjected to Western blot analysis as described in *B*. *E*, confluent and sparse HUVECs were starved in medium 199 containing 1% BSA for 12 h, and treated with 10 μM SB216763 for the periods indicated at the *top* (*h*). Cell lysates were subjected to Western blot analysis with anti-Dll4 (*Dll4*), anti-NICD (*NICD*), and anti-tubulin (*tubulin*) antibodies. *F*, the effect of 20 mM LiCl on the expression of Dll4 and NICD was analyzed as described in *E*. In *C*, a significant difference between two groups is indicated as: *, $p < 0.05$. *n.s.* indicates no significance between two groups.

induced by SB216763 did not occur in the absence of β-catenin (Fig. 4*C*). These results suggest that Ang1 stimulates β-catenin-dependent transcriptional activity through AKT-mediated inhibition of GSK3β, thereby inducing Dll4 expression.

We next investigated whether Ang1 stimulates Dll4 transcription through the TCF-binding site located 706 bp upstream from the transcription initiation site of the mouse

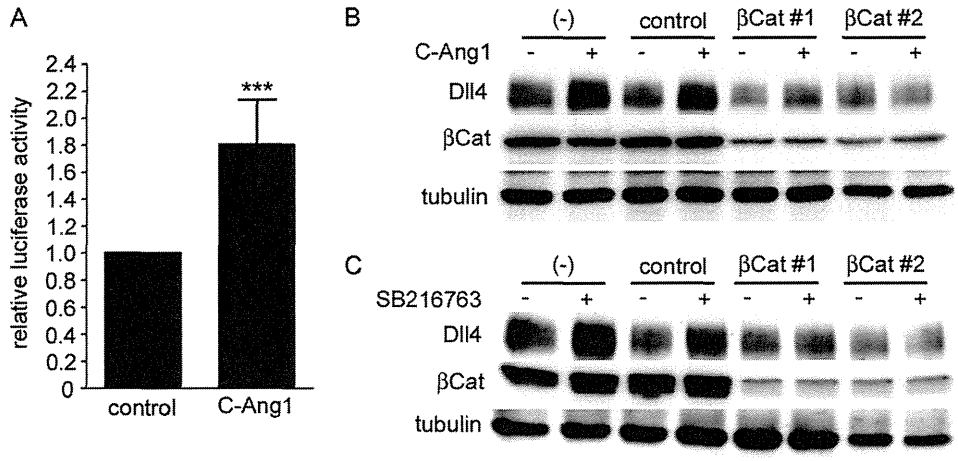

FIGURE 4. **Ang1 induces Dll4 expression through activation of β-catenin.** *A*, confluent HUVECs were transfected with TOPflash reporter plasmid together with pRL-TK vector. After transfection, the cells were starved in medium 199 containing 1% BSA for 4 h, and stimulated with vehicle (*control*) or COMP-Ang1 (*C-Ang1*) for 4 h. After stimulation, the cells were collected, and the lysates were assayed for firefly and *Renilla* luciferase activities as described under "Experimental Procedures." The data represent firefly luciferase activity normalized by the *Renilla* luciferase activity present in each cellular lysate. Values are expressed relative to that observed in the cells treated with vehicle, and shown as mean ± S.D. of four independent experiments. *B*, confluent HUVECs were transfected without (−) or with either control siRNA (*control*) or two independent siRNAs targeting β-catenin (*βCat#1* and *βCat#2*). Then, the cells were starved and stimulated with vehicle (−) or COMP-Ang1 (+) for 1 h. Cell lysates were subjected to Western blot analysis with anti-Dll4 (*Dll4*), anti-β-catenin (*βCat*), and anti-tubulin (*tubulin*) antibodies. *C*, confluent HUVECs transfected with siRNAs as described in *B* were starved, and treated with vehicle (−) or 10 μM SB216763 (+) for 2 h. Cell lysates were subjected to Western blot analysis as described in *B*. In *A*, a significant difference between two groups is indicated as: ***, $p < 0.001$.

Dll4 gene. For that, HUVECs were transfected with the luciferase reporter plasmid in which the reporter is driven by the 3.7-kb mouse Dll4 promoter (Dll4−3.7k-Luc). COMP-Ang1 did not activate the 3.7-kb mouse Dll4 promoter, although Foxc2 significantly stimulated the Dll4−3.7k-Luc reporter activity as previously reported (supplemental Fig. S4, *A* and *B*) (41). However, CA-βCat, an active mutant of β-catenin, did not induce luciferase expression driven by the Dll4−3.7k-Luc reporter gene, although the TOPflash reporter activity was significantly enhanced by CA-βCat (supplemental Fig. S4, *B* and *C*). These results indicate that Ang1 stimulates Dll4 transcription independently of the TCF-binding element located in the proximal Dll4 promoter.

Cell-Cell Contact-dependent Notch Signaling Is Required for Ang1-induced Dll4 Expression—Expression of Dll4 is higher in confluent endothelial cells than in sparse cells (Fig. 1, *C*, *D*, and *G*). In addition, either COMP-Ang1 or GSK3β inhibitor induced Dll4 up-regulation only in the confluent but not sparse endothelial cells (Figs. 1, *A* and *C*, and 3, *E* and *F*). These results imply that the cell-cell contact-dependent signal induces Dll4 expression and is required for β-catenin-mediated Dll4 up-regulation. Recently, Yamamizu *et al.* (47) have reported that β-catenin forms a complex with NICD on the RBP-J binding sites of genes that determine the arterial fate of endothelial cells. Importantly, they also identified the RBP-J binding site within intron 3 of both mouse *Dll4* gene and human *DLL4* gene by performing *in silico* analysis of the cis-acting elements (Fig. 5*A*). These findings prompted us to hypothesize that the Notch signal is a cell-cell contact-dependent signal responsible for Ang1-induced Dll4 expression. To address this possibility, we examined the effect of depletion of NICD by DAPT, a γ-secretase inhibitor, on Ang1-induced Dll4 expression. Treatment of confluent HUVECs with DAPT not only depleted NICD but also reduced basal Dll4 expression. In addition, DAPT prevented COMP-Ang1-induced Dll4 expression and subsequent NICD production (Fig. 5, *B* and *C*). Dll4 up-regulation induced by SB216763 was also inhibited by treatment with DAPT (Fig. 5, *D* and *E*). These results indicate that cell-cell contact-dependent Notch signaling contributes to basal Dll4 expression and is indispensable for Ang1-induced Dll4 up-regulation through β-catenin.

To further investigate whether intron 3 of the *DLL4* gene containing the RBP-J binding site acts as an Ang1-responsive enhancer element, HUVECs were transfected with either a plasmid expressing the luciferase reporter gene under control of the human *DLL4 intron 3* (Dll4-Int3-Luc) or its mutant plasmid in which the RBP-J binding site is mutated (Dll4-Int3mut-Luc) (Fig. 5*A*). COMP-Ang1 significantly stimulated Dll4-Int3-Luc reporter activity, which was inhibited by wortmannin (Fig. 5, *F* and *G*). In contrast, the Dll4-Int3mut-Luc reporter was not activated by COMP-Ang1 (Fig. 5*F*). In addition, inhibition of Notch signaling by DAPT abolished COMP-Ang1-induced activation of the Dll4-Int3-Luc reporter (Fig. 5*H*). These results indicate that Ang1 stimulates the enhancer activity of *DLL4 intron 3* in a Notch signal-dependent manner.

Because β-catenin was essential for Ang1-induced Dll4 expression (Fig. 4*B*), we assumed that β-catenin and NICD might cooperatively stimulate the enhancer activity of the *DLL4 intron 3*. To address this possibility, HUVECs were transfected with either Dll4-Int3-Luc or the Dll4-Int3mut-Luc reporter together with the plasmid encoding CA-βCat and/or that expressing NICD. NICD stimulated Dll4-Int3-Luc but not Dll4-Int3mut-Luc reporter activity (Fig. 5*I*). Although CA-βCat did not stimulate both reporter genes, it potently augmented NICD-stimulated Dll4-Int3-Luc reporter activity (Fig. 5*I*). However, Dll4-Int3mut-Luc reporter activity did not increase even if CA-βCat and NICD were co-expressed (Fig. 5*I*). Collectively, these results indicate that NICD stimulates the enhancer activity of *DLL4 intron 3* via the RBP-J binding site

and that β-catenin potentiates the NICD-induced stimulation of the enhancer activity.

Ang1 Recruits β-Catenin to the NICD·RBP-J Complexes on the Dll4 Intron 3—To understand how β-catenin potentiates Notch signal-mediated Dll4 expression, we examined the complex formation of β-catenin, NICD, and RBP-J on the Dll4 intron 3 enhancer region by performing a ChIP assay. Binding of NICD and RBP-J to the *DLL4 intron 3* was detected in confluent HUVECs irrespective of the presence and absence of COMP-Ang1 (Fig. 6*A*). Although β-catenin did not exist in *DLL4 intron 3* in the unstimulated confluent cells, COMP-Ang1 potently induced binding of β-catenin to the *DLL4 intron 3* (Fig. 6*A*). Together with the results of Dll4-Int3-Luc reporter assays, these findings suggest that the Ang1/Tie2 signal recruits β-catenin to the NICD·RBP-J complexes on Dll4 intron 3. To confirm it, we carried out a co-immunoprecipitation assay using the anti-NICD antibody. Only a small fraction of β-catenin interacted with NICD in confluent HUVECs (Fig. 6*B*). However, stimulation with COMP-Ang1 enhanced the association between β-catenin and NICD without affecting the expression of Dll4 and NICD (Fig. 6*B*). Collectively, these findings indicate that the Ang1/

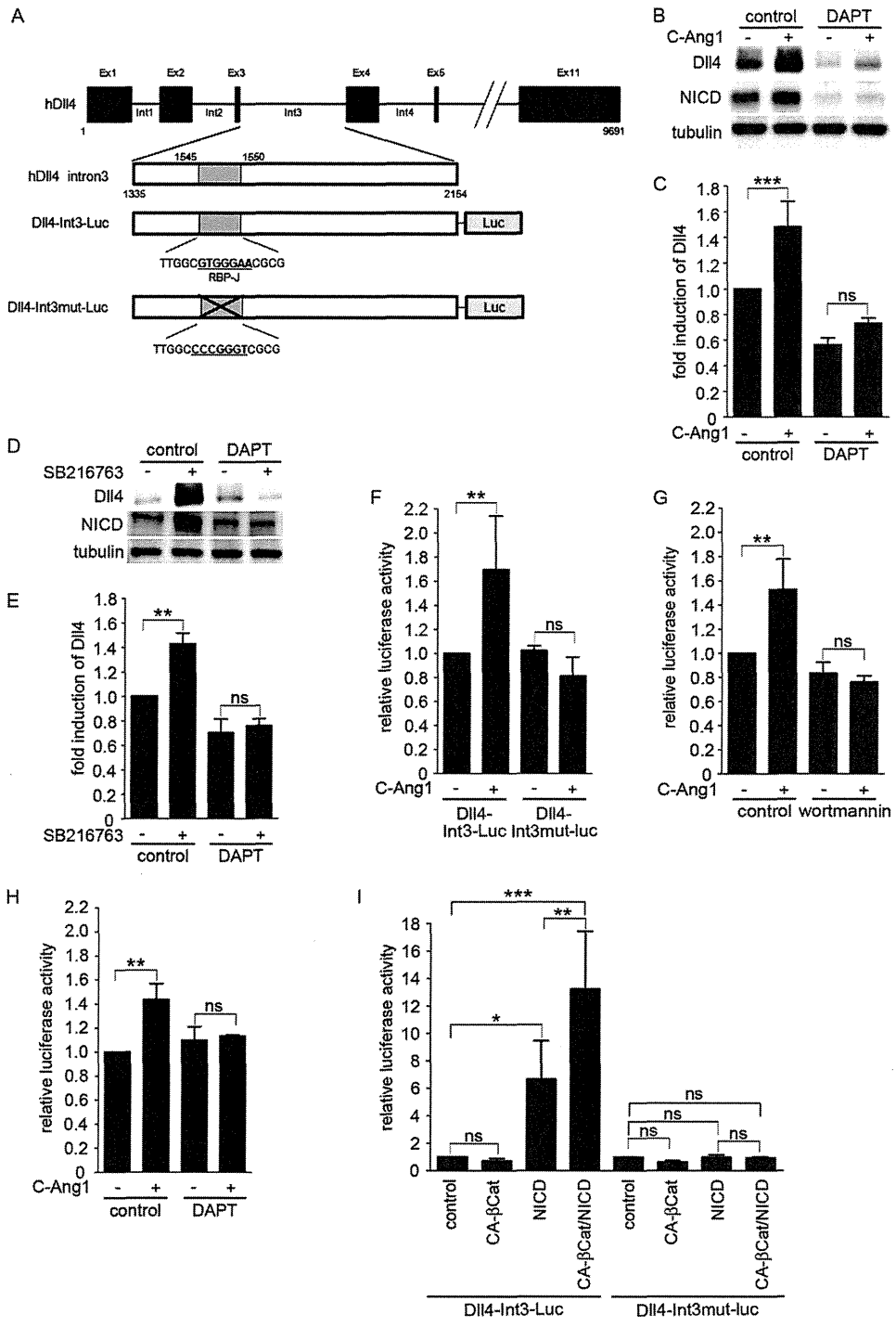

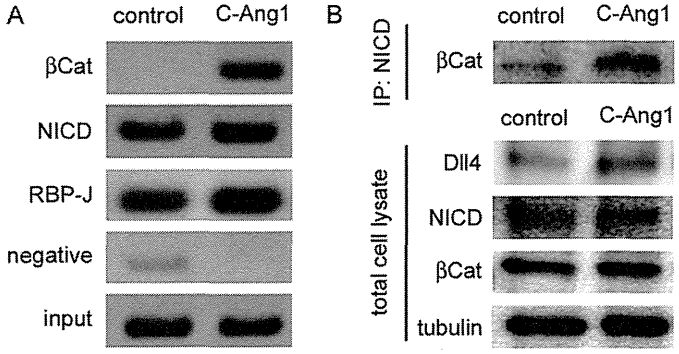

FIGURE 6. **β-Catenin is recruited to the NICD·RBP-J complexes on Dll4 intron 3 in response to Ang1.** *A*, confluent HUVECs starved for 12 h were stimulated with vehicle (control) or COMP-Ang1 (*C-Ang1*) for 30 min. After stimulation, the cells were fixed with formaldehyde, and the cross-linked chromatin was immunoprecipitated with anti-β-catenin (*βCat*), anti-NICD (*NICD*), anti-RBP-J (*RBP-J*), and control (*negative*) antibodies. Input (*input*) and co-immunoprecipitated DNA were used as a template for PCR amplification. PCR amplification was performed using the primers specifically targeting Dll4 intron 3. *B*, confluent HUVECs starved for 12 h were stimulated with COMP-Ang1 as described in *A*. Cell lysates were immunoprecipitated with anti-NICD antibody. Immunoprecipitates (*IP: NICD*) and aliquots of cell lysates (*total cell lysate*) were subjected to Western blot analysis with anti-β-catenin (*βCat*), anti-Dll4 (*Dll4*), anti-NICD (*NICD*), and anti-tubulin (*tubulin*) antibodies as indicated at the *left*.

Tie2 signal recruits β-catenin to the NICD·RBP-J complexes on the enhancer region of Dll4 intron 3, thereby inducing Dll4 up-regulation.

Ang1 Induces Extracellular Deposition of Collagen Type IV through Dll4/Notch Signaling—Both Ang1/Tie2 and Dll4/Notch signaling are known to induce formation of the vascular basement membrane (33, 36, 37), which is a hallmark of vascular stabilization. Therefore, we investigated whether Ang1 induces deposition of collagen type IV, a major basement membrane component, during endothelial cell tube formation in three-dimensional collagen matrices. Extracellular deposition of collagen type IV was markedly increased by stimulation with COMP-Ang1 (Fig. 7, *A* and *B*). However, inhibition of Notch signaling by treatment with DAPT inhibited COMP-Ang1-induced deposition of collagen type IV (Fig. 7, *A* and *B*). Consistently, collagen type IV deposition was not induced by COMP-Ang1 in Dll4-depleted cells (Fig. 7*C* and supplemental Fig. S5). These findings suggest that Ang1 induces basement membrane formation through Dll4/Notch signaling.

DISCUSSION

We here explored how Ang1 induces Dll4 expression and suggested its contribution to Ang1-regulated vascular quiescence. Ang1 assembles distinct Tie2 signaling complexes in the presence or absence of cell-cell junctions, thereby regulating both vascular quiescence and angiogenesis. In the presence of cell-cell junctions, Ang1 induces formation of *trans*-associated Tie2, which induces expression of the genes involved in vascular stabilization, which include Notch ligand Dll4. Because the Dll4/Notch signal is known to restrict sprouting angiogenesis and promote vascular stabilization (15, 17–21, 30, 31), we hypothesized that the Dll4/Notch signal is involved in Ang1/Tie2 signal-mediated vascular quiescence. To address this possibility, we decided to delineate the signaling pathways underlying Ang1-induced Dll4 expression. We found that the Ang1/Tie2 signal induces activation of β-catenin through AKT-mediated inhibition of GSK3β and that β-catenin resistant to degradation enhances Notch signal-mediated Dll4 expression by forming a complex with NICD/RBP-J on the RBP-J binding site in Dll4 intron 3, thereby potentiating the Dll4/Notch signal leading to vascular quiescence (Fig. 7).

Basal Dll4 expression and NICD is higher in confluent cells than in the sparse cells (Fig. 1*G*), consistent with the previous report that cell-cell contact-dependent Notch signaling induces Dll4 expression (48). Importantly, either Ang1- or GSK3β inhibitor-induced Dll4 expression requires endothelial cell-cell contacts, and is sensitive to DAPT, suggesting that Notch signaling is a prerequisite for β-catenin-mediated Dll4 expression.

Augmentation of Dll4 expression by Ang1 is dependent on β-catenin. We have previously shown that the Ang1/Tie2 signal preferentially activates PI3K/AKT signaling (10). Although phosphorylation of β-catenin by GSK3β leads to its degradation, β-catenin is stabilized by inhibition of GSK3β by AKT.

FIGURE 5. **Ang1 stimulates the enhancer activity of the *DLL4* intron 3 in a Notch signal-dependent manner.** *A*, the exon-intron organization of the human *DLL4* gene and the structures of luciferase reporter constructs. Note that human *DLL4 intron 3* contains the RBP-J binding site. The Dll4-Int3-Luc reporter plasmid expresses the firefly luciferase reporter gene under control of the human *DLL4 intron 3*. In the Dll4-Int3mut-Luc reporter construct, the RBP-J binding site is disrupted. *B*, confluent HUVECs starved for 12 h were pretreated with vehicle (*control*) or 10 μM DAPT for 8 h, and subsequently stimulated with vehicle (−) or COMP-Ang1 (+) for 1 h. Western blot analysis was performed as described in the legend of Fig. 1*G*. *C*, the expression of Dll4 observed in *B* are quantified as described in legend of Fig. 1*D*. Values are expressed as fold-induction relative to that in the DAPT-untreated cells stimulated with vehicle, and shown as mean ± S.D. of five independent experiments. *D*, confluent HUVECs pretreated with DAPT as described in *B* were stimulated with vehicle (−) or SB216763 (+) for 2 h. Western blot analysis was performed as described in *B*. *E*, the expression of Dll4 observed in *D* are quantified as described in legend of Fig. 1*D*. Values are expressed as described in *C*, and shown as mean ± S.D. of 4 independent experiments. *F*, confluent HUVECs transfected with either Dll4-Int3-Luc or Dll4-Int3mut-Luc reporter constructs together with pRL-SV40 vector were starved in medium 199 containing 1% BSA for 12 h, and stimulated with vehicle (*control*) or COMP-Ang1 (+) for 3 h. After the stimulation, the cells were collected, and the lysates were assayed for firefly and *Renilla* luciferase activities as described in the legend of Fig. 4*A*. Values are expressed relative to that observed in control cells expressing the Dll4-Int3-Luc plasmid, and shown as mean ± S.D. of three independent experiments. *G*, confluent HUVECs co-transfected with the Dll4-Int3-Luc reporter plasmid and pRL-SV40 vector were starved in medium 199 containing 1% BSA for 12 h, pretreated with vehicle (*control*) or 60 nM wortmannin for 30 min, and stimulated with vehicle (−) or COMP-Ang1 (+) for 3 h. After stimulation, the cells were collected, and the lysates were assayed for firefly and *Renilla* luciferase activities as described in the legend of Fig. 4*A*. Values are expressed relative to that observed in the wortmannin-untreated cells stimulated with vehicle, and shown as mean ± S.D. of four independent experiments. *H*, confluent HUVECs co-expressing both Dll4-Int3-Luc plasmid and pRL-SV40 vector were starved for 12 h, pretreated with vehicle (*control*) or 10 μM DAPT for 1 h, and stimulated with vehicle (−) or COMP-Ang1 (+) for 3 h. Firefly and *Renilla* luciferase activities were assayed as described in the legend of Fig. 4*A*. Values are expressed relative to that in the DAPT-untreated cells stimulated with vehicle, and shown as mean ± S.D. of three independent experiments. *I*, confluent HUVECs were transfected with either Dll4-Int3-Luc or Dll4-Int3mut-Luc reporter construct together with pRL-SV40 vector and the empty vector (*control*) or the plasmid encoding either CA-βCat or NICD. Cell lysates were assayed for firefly and *Renilla* luciferase activities as described in the legend of Fig. 4*A*. Values are expressed relative to that observed in the control cells expressing the Dll4-Int3-Luc reporter plasmid, and shown as mean ± S.D. of five independent experiments. Significant differences between two groups (*C* and *E–I*) are indicated as: *, $p < 0.05$; **, $p < 0.01$; ***, $p < 0.001$. *n.s.* indicates no significance between two groups.

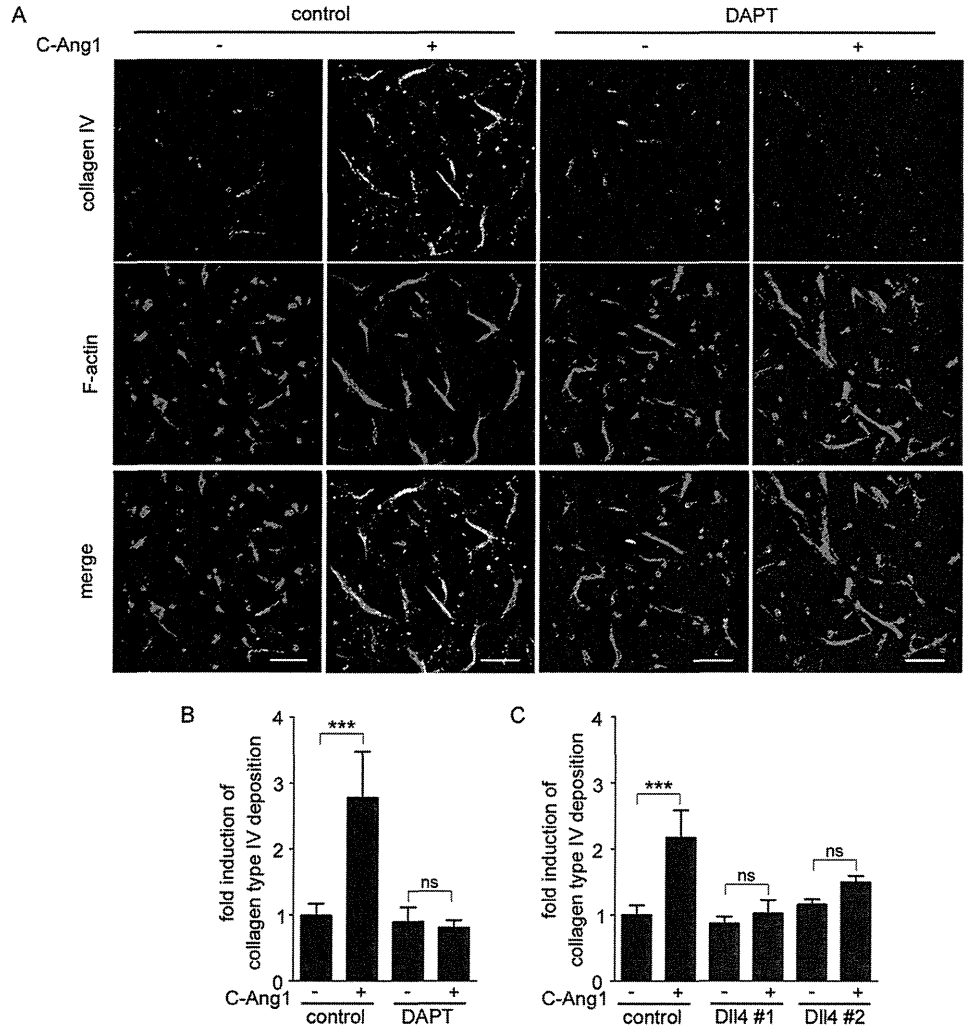

FIGURE 7. **Ang1 induces extracellular deposition of collagen type IV via Dll4/Notch signaling.** *A*, HUVECs were cultured to form tube structures in three-dimensional collagen matrices for 48 h. During this period, the cells were stimulated with vehicle (−) or COMP-Ang1 (+) in the presence (*DAPT*) or absence (*control*) of 20 μM DAPT as indicated at the *top*. To detect the extracellular deposition of collagen type IV, the cultures were fixed, immunostained with anti-collagen type IV antibody, and visualized with Alexa 488-conjugated secondary antibody. After permeabilization, the cells were further stained with rhodamine-phalloidin to visualize filamentous actin. Alexa 488 and rhodamine images were obtained through a confocal microscope. Alexa 488 (*collagen IV*) and rhodamine (*F-actin*) images and the merged images (*merge*) are shown as indicated at the *left*. *Scale bar*, 100 μm. *B*, extracellular deposition of collagen type IV was quantified as described under "Experimental Procedures." Values are expressed as fold-induction relative to that observed in DAPT-untreated cells stimulated with vehicle, and shown as mean ± S.D. of five different fields. Similar results were obtained in four independent experiments. *C*, HUVECs transfected with either control siRNA (*control*) or two independent siRNAs targeting Dll4 (*Dll4#1* and *Dll4#2*) were cultured to form tube structures in three-dimensional collagen matrices for 48 h. During this period, the cells were stimulated with vehicle (−) or COMP-Ang1 (+) as indicated at the *bottom*. The extracellular deposition of collagen type IV was detected and quantified as described in *A* and *B*. Values are expressed as fold-induction relative to that observed in control siRNA-transfected cells stimulated with vehicle, and shown as mean ± S.D. of five different fields. In *B* and *C*, significant differences between two groups are indicated as: ***, $p < 0.001$. *n.s.* indicates no significance between two groups.

Dll4 expression by Ang1 was inhibited by depletion of β-catenin and inhibition of either PI3K or AKT (Figs. 2, *A–D*, and 4*B*), indicating the essential role of β-catenin for Ang1-induced Dll4 expression. Thus, we further extend the study on the transcriptional regulation of Dll4 by β-catenin.

We first analyzed the −3.7-kb promoter region of the mouse *Dll4* gene, because this region contains transcription factor binding sites for forkhead transcription factors and TCF. The forkhead transcription factors, Foxc1 and Foxc2, are the first transcription factors identified to regulate Dll4 expression during vascular development (41). Mouse embryos deficient in both Foxc1 and Foxc2 exhibit arteriovenous malformation and lack of expression of arterial genes, such as *Dll4* and *ephrinB2*. Consistently, Foxc1 and Foxc2 directly activate the Dll4 promoter via the forkhead binding element located ~3.7 kb upstream from the transcription initiation site (41). Thus, Dll4 induction responsible for arterial-venous cell fate determination appears to be mediated by *Foxc* genes. However, Ang1 did not stimulate the −3.7-kb Dll4 promoter containing the forkhead binding element, suggesting that Foxc1 and Foxc2 are not involved in Ang1-induced Dll4 expression. In addition, Corada *et al.* (46) have recently reported that β-catenin up-regulates Dll4 transcription through the TCF-binding site located 706 bp upstream from the transcription initiation site of the mouse *Dll4* gene. However, in our experiments, neither Ang1 nor CA-βCat activated the −3.7-kb mouse Dll4 promoter containing the corresponding TCF binding site. Instead, our luciferase reporter assays and ChIP experiments performed in this study

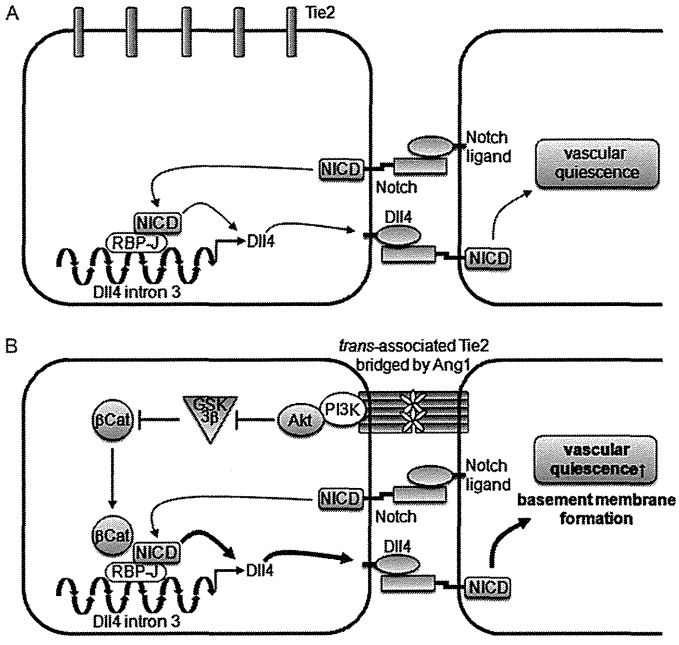

FIGURE 8. **Schematic representation of a proposed model for how Ang1/Tie2 signal induces Dll4 expression to potentiate Notch signal.** *A*, in the confluent endothelial cells, cell-cell contact-dependent Notch signaling induces production of NICD, which subsequently binds to the RBP-J binding site in Dll4 intron 3, leading to Dll4 expression. *B*, in confluent cells, the Ang1/Tie2 signal stimulates the transcriptional activity of β-catenin through the PI3K/AKT pathway-mediated inhibition of GSK3β. The stabilized β-catenin enhances NICD-mediated Dll4 expression by forming a complex with NICD and RBP-J on Dll4 intron 3, which augments the Notch signal. Dll4/Notch signal augmented by the Ang1/Tie2 signal promotes formation of vascular basement membrane leading to vascular quiescence. In the absence of cell-cell contacts, Dll4 expression is very low due to the lack of Notch signaling. Even if the cells are stimulated with Ang1 under this condition, Dll4 up-regulation does not occur, because the Ang1/Tie2 signal is unable to induce Dll4 expression in the absence of Notch signaling (not described in this figure).

revealed that Dll4 intron 3 is an enhancer element responsible for Ang1-induced Dll4 transcription through β-catenin. Currently, the reason for this discrepancy remains unclear, but it may be due to the different cell types used for the experiments. We performed the experiments with HUVECs, whereas they used endothelial cells isolated from mouse embryos (46). Consistent with this idea, VEGF-induced Dll4 expression occurs only in arterial endothelial cell, but not in venous cells (49). Thus, the signaling pathways leading to Dll4 expression may vary in different endothelial cell types and in different upstream mediators.

Ang1 induces recruitment of β-catenin to NICD·RBP-J complexes on the RBP-J binding site in Dll4 intron 3, which enhances NICD-mediated Dll4 expression. Thus, Ang1/Tie2 and Notch signaling converges into β-catenin·NICD·RBP-J complexes on the Dll4 intron 3 enhancer to cooperatively induce Dll4 expression. Consistently, functional interaction between NICD and β-catenin has recently been reported (47, 50). In arterial, but not venous, endothelial cells, β-catenin·NICD·RBP-J complexes are formed on the RBP-J binding sites of arterial genes, thereby regulating their expression leading to arterial fate specification (47). In addition, it has also been shown that β-catenin·NICD·RBP-J complexes on the Hes1 promoter induce Hes1 expression to suppress the differentiation of neural precursor cells (50). Thus, the functional interaction between Notch and β-catenin signaling may be involved in a variety of biological processes.

Both Ang1/Tie2 and Notch signal are known to regulate vascular quiescence. Functional similarity between them and our present evidence that Ang1 induces Dll4 expression leading to Notch activation imply the role of the Dll4/Notch signal in Ang1/Tie2-mediated vascular quiescence. We further revealed that Ang1 induces extracellular deposition of collagen type IV, a major component of basement membrane, during endothelial cell tube formation. This Ang1-mediated deposition of collagen type IV is dependent of the Dll4/Notch signal, as demonstrated by evidence that inhibition of the Notch signal by DAPT and deletion of Dll4 by siRNA prevented this effect (Fig. 7). Because basement membrane matrix assembly is a crucial step for vascular maturation and stabilization (51), these findings suggest that the Ang1/Tie2 signal might promote vascular stabilization through activation of Dll4/Notch signal.

The Dll4/Notch signal is also involved in tip/stalk cell specification (15). Activation of the Notch signal in the stalk cells restricts their angiogenic behavior, thereby maintaining a quiescent and stabilized phenotype of stalk cells. Interestingly, Yana *et al.* (37) have found by using an *ex vivo* angiogenesis system that Tie2 is specifically expressed in stalk cells and is involved in vessel maturation. Thus, the Ang1/Tie2 signal may also regulate Dll4 expression in the stalk cells, leading to the maturation of neovessels. However, the *in vivo* study must be required to clarify the role of cross-talk between the Ang1/Tie2 and Dll4/Notch signal in vascular stabilization.

In conclusion, we found that the Ang1/Tie2 signal induces activation of β-catenin through the PI3K/AKT pathway-mediated inhibition of GSK3β in the presence of cell-cell contacts, and that the undegraded β-catenin subsequently potentiates the Notch signal-mediated Dll4 expression by forming a complex with NICD/RBP-J on the RBP-J binding site in Dll4 intron 3, which in turn up-regulates the Dll4/Notch signal. In addition, we also revealed that the Dll4/Notch signal augmented by the Ang1/Tie2 signal promotes formation of vascular basement membrane leading to vascular stabilization (Fig. 8).

Acknowledgments—We are grateful to J. S. Gutkind (National Institute of Health) for the CA-βCat plasmid, M. Kurabayashi (Gunma University) for the Notch1 ICD plasmid, M. Matsuda (Kyoto University) and Y. Fujio (Osaka University) for the adenovirus encoding LacZ and CA-AKT, respectively. We also thank K. Hiratomi, M. Sone, M. Minamimoto, and Y. Matsuura for technical assistance, and N. Takakura (Osaka University), J. K. Yamashita (Kyoto University), K. Yamamizu (Kyoto University), and M. Masuda for helpful advice.

REFERENCES

1. Dumont, D. J., Gradwohl, G., Fong, G. H., Puri, M. C., Gertsenstein, M., Auerbach, A., and Breitman, M. L. (1994) *Genes Dev.* **8**, 1897–1909
2. Sato, T. N., Tozawa, Y., Deutsch, U., Wolburg-Buchholz, K., Fujiwara, Y., Gendron-Maguire, M., Gridley, T., Wolburg, H., Risau, W., and Qin, Y. (1995) *Nature* **376**, 70–74
3. Suri, C., Jones, P. F., Patan, S., Bartunkova, S., Maisonpierre, P. C., Davis, S., Sato, T. N., and Yancopoulos, G. D. (1996) *Cell* **87**, 1171–1180
4. Brindle, N. P., Saharinen, P., and Alitalo, K. (2006) *Circ. Res.* **98**, 1014–1023
5. Peters, K. G., Kontos, C. D., Lin, P. C., Wong, A. L., Rao, P., Huang, L.,

Dewhirst, M. W., and Sankar, S. (2004) *Recent Prog. Horm. Res.* **59,** 51–71
6. Wong, A. L., Haroon, Z. A., Werner, S., Dewhirst, M. W., Greenberg, C. S., and Peters, K. G. (1997) *Circ. Res.* **81,** 567–574
7. Asahara, T., Chen, D., Takahashi, T., Fujikawa, K., Kearney, M., Magner, M., Yancopoulos, G. D., and Isner, J. M. (1998) *Circ. Res.* **83,** 233–240
8. Eklund, L., and Olsen, B. R. (2006) *Exp. Cell Res.* **312,** 630–641
9. Lin, P., Polverini, P., Dewhirst, M., Shan, S., Rao, P. S., and Peters, K. (1997) *J. Clin. Invest.* **100,** 2072–2078
10. Fukuhara, S., Sako, K., Minami, T., Noda, K., Kim, H. Z., Kodama, T., Shibuya, M., Takakura, N., Koh, G. Y., and Mochizuki, N. (2008) *Nat. Cell. Biol.* **10,** 513–526
11. Saharinen, P., Eklund, L., Miettinen, J., Wirkkala, R., Anisimov, A., Winderlich, M., Nottebaum, A., Vestweber, D., Deutsch, U., Koh, G. Y., Olsen, B. R., and Alitalo, K. (2008) *Nat. Cell. Biol.* **10,** 527–537
12. Sako, K., Fukuhara, S., Minami, T., Hamakubo, T., Song, H., Kodama, T., Fukamizu, A., Gutkind, J. S., Koh, G. Y., and Mochizuki, N. (2009) *J. Biol. Chem.* **284,** 5592–5601
13. Artavanis-Tsakonas, S., Rand, M. D., and Lake, R. J. (1999) *Science* **284,** 770–776
14. Gridley, T. (1997) *Mol. Cell. Neurosci.* **9,** 103–108
15. Phng, L. K., and Gerhardt, H. (2009) *Dev. Cell* **16,** 196–208
16. Iso, T., Kedes, L., and Hamamori, Y. (2003) *J. Cell. Physiol.* **194,** 237–255
17. Hellström, M., Phng, L. K., Hofmann, J. J., Wallgard, E., Coultas, L., Lindblom, P., Alva, J., Nilsson, A. K., Karlsson, L., Gaiano, N., Yoon, K., Rossant, J., Iruela-Arispe, M. L., Kalén, M., Gerhardt, H., and Betsholtz, C. (2007) *Nature* **445,** 776–780
18. Leslie, J. D., Ariza-McNaughton, L., Bermange, A. L., McAdow, R., Johnson, S. L., and Lewis, J. (2007) *Development* **134,** 839–844
19. Lobov, I. B., Renard, R. A., Papadopoulos, N., Gale, N. W., Thurston, G., Yancopoulos, G. D., and Wiegand, S. J. (2007) *Proc. Natl. Acad. Sci. U.S.A.* **104,** 3219–3224
20. Siekmann, A. F., and Lawson, N. D. (2007) *Nature* **445,** 781–784
21. Suchting, S., Freitas, C., le Noble, F., Benedito, R., Bréant, C., Duarte, A., and Eichmann, A. (2007) *Proc. Natl. Acad. Sci. U.S.A.* **104,** 3225–3230
22. Williams, C. K., Li, J. L., Murga, M., Harris, A. L., and Tosato, G. (2006) *Blood* **107,** 931–939
23. Li, J. L., Sainson, R. C., Shi, W., Leek, R., Harrington, L. S., Preusser, M., Biswas, S., Turley, H., Heikamp, E., Hainfellner, J. A., and Harris, A. L. (2007) *Cancer Res.* **67,** 11244–11253
24. Noguera-Troise, I., Daly, C., Papadopoulos, N. J., Coetzee, S., Boland, P., Gale, N. W., Lin, H. C., Yancopoulos, G. D., and Thurston, G. (2006) *Nature* **444,** 1032–1037
25. Ridgway, J., Zhang, G., Wu, Y., Stawicki, S., Liang, W. C., Chanthery, Y., Kowalski, J., Watts, R. J., Callahan, C., Kasman, I., Singh, M., Chien, M., Tan, C., Hongo, J. A., de Sauvage, F., Plowman, G., and Yan, M. (2006) *Nature* **444,** 1083–1087
26. Augustin, H. G., Koh, G. Y., Thurston, G., and Alitalo, K. (2009) *Nat. Rev. Mol. Cell Biol.* **10,** 165–177
27. Falcón, B. L., Hashizume, H., Koumoutsakos, P., Chou, J., Bready, J. V., Coxon, A., Oliner, J. D., and McDonald, D. M. (2009) *Am. J. Pathol.* **175,** 2159–2170
28. Hawighorst, T., Skobe, M., Streit, M., Hong, Y. K., Velasco, P., Brown, L. F., Riccardi, L., Lange-Asschenfeldt, B., and Detmar, M. (2002) *Am. J. Pathol.* **160,** 1381–1392
29. Machein, M. R., Knedla, A., Knoth, R., Wagner, S., Neuschl, E., and Plate, K. H. (2004) *Am. J. Pathol.* **165,** 1557–1570
30. Phng, L. K., Potente, M., Leslie, J. D., Babbage, J., Nyqvist, D., Lobov, I., Ondr, J. K., Rao, S., Lang, R. A., Thurston, G., and Gerhardt, H. (2009) *Dev. Cell* **16,** 70–82
31. Dou, G. R., Wang, Y. C., Hu, X. B., Hou, L. H., Wang, C. M., Xu, J. F., Wang, Y. S., Liang, Y. M., Yao, L. B., Yang, A. G., and Han, H. (2008) *FASEB J.* **22,** 1606–1617
32. Fukuhara, S., Sako, K., Noda, K., Zhang, J., Minami, M., and Mochizuki, N. (2010) *Histol. Histopathol.* **25,** 387–396
33. Benedito, R., Trindade, A., Hirashima, M., Henrique, D., da Costa, L. L., Rossant, J., Gill, P. S., and Duarte, A. (2008) *BMC Dev. Biol.* **8,** 117
34. Iivanainen, E., Nelimarkka, L., Elenius, V., Heikkinen, S. M., Junttila, T. T., Sihombing, L., Sundvall, M., Maatta, J. A., Laine, V. J., Yla-Herttuala, S., Higashiyama, S., Alitalo, K., and Elenius, K. (2003) *FASEB J.* **17,** 1609–1621
35. Kobayashi, H., DeBusk, L. M., Babichev, Y. O., Dumont, D. J., and Lin, P. C. (2006) *Blood* **108,** 1260–1266
36. Trindade, A., Kumar, S. R., Scehnet, J. S., Lopes-da-Costa, L., Becker, J., Jiang, W., Liu, R., Gill, P. S., and Duarte, A. (2008) *Blood* **112,** 1720–1729
37. Yana, I., Sagara, H., Takaki, S., Takatsu, K., Nakamura, K., Nakao, K., Katsuki, M., Taniguchi, S., Aoki, T., Sato, H., Weiss, S. J., and Seiki, M. (2007) *J. Cell Sci.* **120,** 1607–1614
38. Cho, C. H., Kammerer, R. A., Lee, H. J., Steinmetz, M. O., Ryu, Y. S., Lee, S. H., Yasunaga, K., Kim, K. T., Kim, I., Choi, H. H., Kim, W., Kim, S. H., Park, S. K., Lee, G. M., and Koh, G. Y. (2004) *Proc. Natl. Acad. Sci. U.S.A.* **101,** 5547–5552
39. Fukuhara, S., Sakurai, A., Sano, H., Yamagishi, A., Somekawa, S., Takakura, N., Saito, Y., Kangawa, K., and Mochizuki, N. (2005) *Mol. Cell. Biol.* **25,** 136–146
40. Aoki, K., Nakamura, T., Fujikawa, K., and Matsuda, M. (2005) *Mol. Biol. Cell* **16,** 2207–2217
41. Seo, S., Fujita, H., Nakano, A., Kang, M., Duarte, A., and Kume, T. (2006) *Dev. Biol.* **294,** 458–470
42. Fukuhara, S., Marinissen, M. J., Chiariello, M., and Gutkind, J. S. (2000) *J. Biol. Chem.* **275,** 21730–21736
43. Koh, W., Stratman, A. N., Sacharidou, A., and Davis, G. E. (2008) *Methods Enzymol.* **443,** 83–101
44. Frame, S., and Cohen, P. (2001) *Biochem. J.* **359,** 1–16
45. Wu, D., and Pan, W. (2010) *Trends Biochem. Sci.* **35,** 161–168
46. Corada, M., Nyqvist, D., Orsenigo, F., Caprini, A., Giampietro, C., Taketo, M. M., Iruela-Arispe, M. L., Adams, R. H., and Dejana, E. (2010) *Dev. Cell* **18,** 938–949
47. Yamamizu, K., Matsunaga, T., Uosaki, H., Fukushima, H., Katayama, S., Hiraoka-Kanie, M., Mitani, K., and Yamashita, J. K. (2010) *J. Cell Biol.* **189,** 325–338
48. Benedito, R., Roca, C., Sörensen, I., Adams, S., Gossler, A., Fruttiger, M., and Adams, R. H. (2009) *Cell* **137,** 1124–1135
49. Liu, Z. J., Shirakawa, T., Li, Y., Soma, A., Oka, M., Dotto, G. P., Fairman, R. M., Velazquez, O. C., and Herlyn, M. (2003) *Mol. Cell. Biol.* **23,** 14–25
50. Shimizu, T., Kagawa, T., Inoue, T., Nonaka, A., Takada, S., Aburatani, H., and Taga, T. (2008) *Mol. Cell. Biol.* **28,** 7427–7441
51. Davis, G. E., and Senger, D. R. (2005) *Circ. Res.* **97,** 1093–1107

THE JOURNAL OF BIOLOGICAL CHEMISTRY VOL. 286, NO. 51, pp. 44243–44253, December 23, 2011

Author's Choice

EphrinA1-EphA2 Signal Induces Compaction and Polarization of Madin-Darby Canine Kidney Cells by Inactivating Ezrin through Negative Regulation of RhoA*[S]

Received for publication, June 1, 2011, and in revised form, October 3, 2011 Published, JBC Papers in Press, October 6, 2011, DOI 10.1074/jbc.M111.267047

Yuki Wakayama[‡], Koichi Miura[‡1], Hisataka Sabe[§], and Naoki Mochizuki[‡2]

From the [‡]Department of Cell Biology, National Cerebral and Cardiovascular Center Research Institute, 5-7-1 Fujishirodai, Suita, Osaka, 565-8565, Japan and the [§]Department of Molecular Biology, Hokkaido University Graduate School of Medicine, Kita-ku, Sapporo, 060-8638, Japan

Background: Molecular mechanism underlying cell-cell contact-dependent cell shape change has remained elusive.
Results: The activation of EphrinA1/EphA2 results in dephosphorylation of Ezrin through the phosphorylation of p190RhoGAP-A.
Conclusion: Ezrin at the apical domain regulates the cell shape and is regulated by ephrinA1/EphA2 signaling upon cell-cell contacts.
Significance: Exploring the molecular mechanism underlying cell shape change contributes to the understanding epithelial-mesenchymal transition.

The epithelial cells exhibit either a columnar or a flat shape dependent on extracellular stimuli or the cell-cell adhesion. Membrane-anchored ephrinA stimulates EphA receptor tyrosine kinases as a ligand in a cell-cell contact-dependent manner. The mechanism through which ephrinA1/EphA2 signal regulates the cell morphology remains elusive. We demonstrate here that ephrinA1/EphA2 signal induces compaction and enhanced polarization (columnar change) of Madin-Darby canine kidney epithelial cells by regulating Ezrin, a linker that connects plasma membrane and actin cytoskeleton. Activation of EphA2 resulted in RhoA inactivation through p190RhoGAP-A and subsequent dephosphorylation of Ezrin on Thr-567 phosphorylated by Rho kinase. Consistently, the cells expressing an active mutant of Ezrin in which Thr-567 was replaced with Asp did not change their shape in response to ephrinA1. Furthermore, depletion of Ezrin led to compaction and enhanced polarization without ephrinA1 stimulation, suggesting the role for active Ezrin in keeping the flat cell shape. Ezrin localized to apical domain irrespective of ephrinA1 stimulation, whereas phosphorylated Ezrin on the apical domain was reduced by ephrinA1 stimulation. Collectively, ephrinA1/EphA2 signal negatively regulates Ezrin and promotes the alteration of cell shape, from flat to columnar shape.

Epithelial cells dynamically reorganize their morphology in response to extracellular signals, during embryogenesis, wound healing, and other biological processes (1, 2). These cell morphological changes are observed as epithelial-mesenchymal transition and its reverse process (mesenchymal-epithelial transition) (3, 4). Epithelial cells have firm adhesions to their neighboring cells to establish cell-cell contact by homophilic association of epithelial cell-cadherin (E-cadherin) supported by actin cytoskeleton and preserve apical to basolateral polarity at the cell-cell contacts (5). When the cells lose the cell-cell contacts and polarity, they transit to mesenchymal cells. However, even in the epithelial state, they change their morphology: between fully columnar shape and flat cell shape with cell-cell adhesions (6). Although the columnar epithelial cells are characterized by the full compaction and enhanced polarization, the flat cells are characterized by the decreased lateral domain with subtle E-cadherin-dependent cell-cell junctions. However, it is not fully understood how epithelial cells change their shape. Not only extracellular stimuli but also cell-cell adhesion molecules that regulate actin cytoskeleton are involved in these morphological changes.

Ezrin is a member of the Ezrin/Radixin/Moesin (ERM)[3] family that regulates actin cytoskeleton by linking plasma membrane proteins, including CD44, Podoplanin, and Podocalyxin/gp135 to cell cortical actin fibers (7–11). Ezrin does not directly regulate the apical to basolateral polarity; however, it is indirectly involved in regulation of cell morphology by binding to actin (7, 8). Ezrin is thought to be folded in an inactive form through an intramolecular interaction between its NH_2-terminal domain and the COOH-terminal domain. Ezrin becomes active by binding to phosphatidylinositol 4,5-bisphosphate (PIP_2) and by being phosphorylated at Thr-567 by Rho kinase, protein kinase C, or NF-κB-inducing kinase (7, 8, 12–15). The unfolded active Ezrin can finally bind to both actin cytoskeleton

* This work was supported in part by grants from the Ministry of Education, Science, Sports and Culture of Japan (to N. M.); the Ministry of Health, Labour, and Welfare of Japan (to N. M.); Takeda Science Foundation (to N. M.); the Mitsubishi Foundation (to N. M.); and an AstraZeneca Research Grant (to N. M.).
Author's Choice—Final version full access.
[S] The on-line version of this article (available at http://www.jbc.org) contains supplemental Figs. S1–S3.
[1] To whom correspondence may be addressed. Tel.: 81-6-6833-5012; Fax: 81-6-6835-5461; E-mail: miurako@ri.ncvc.go.jp.
[2] To whom correspondence may be addressed. Tel.: 81-6-6833-5012; Fax: 81-6-6835-5461; E-mail: nmochizu@ri.ncvc.go.jp.

[3] The abbreviations used are: ERM, Ezrin/Radixin/Moesin; Arf6, ADP-ribosylation factor 6; E-cadherin, epithelial cell-cadherin; GAP, GTPase-activating protein; MDCK, Madin-Darby canine kidney; PIP_2, phosphatidylinositol 4,5-bisphosphate; PIP5K, phosphatidylinositol 4-phosphate 5-kinase.

and plasma membrane proteins to function at the apical cell membrane. It is still unclear how Ezrin is dephosphorylated, although increased cell density of endothelial cells leads to dephosphorylation of ERM, probably by cell-cell contact-dependent signal (16).

EphA and EphB (erythropoietin-producing hepatocellular carcinoma A and B) tyrosine kinase receptors are activated by binding to their ligands, ephrinA anchored to the plasma membrane and ephrinB passing the membrane, respectively (17). Thus, Eph receptor signals extracellular stimulus to the inside of the cells in a manner dependent on cell-cell contacts. Among EphA receptors (EphA1–EphA8 and EphA10), EphA2 is expressed in various cells including epithelial cells and endothelial cells (18, 19). Because ephrinA1 is similarly expressed in epithelial and endothelial cells to EphA2, ephrinA1 induces EphA2 activation upon cell-cell contacts. We previously reported that activation of EphA2 by ephrinA1 induces compaction and enhanced polarization of Madin-Darby canine kidney (MDCK) epithelial cells (20). This morphological change is ascribed to an inactivation of ADP-ribosylation factor 6 (Arf6) by EphA2-Nck1-Git1 pathway. Our data suggested that there might be other signaling pathways besides inactivation of Arf6 in ephrinA1-induced cell compaction. In MDCK cells, ectopic expression of Podoplanin induces epithelial-mesenchymal transition through the activation of Ezrin and RhoA (21), indicating an involvement of Ezrin in flattening of the cells lacking cell-cell contacts. Therefore, ephrinA1/EphA2 might counteract or negatively regulate Ezrin-controlled cell shape change.

Apical to basolateral polarity is well maintained in the columnar cells (5). Increased height of lateral domain is shown by an increase in E-cadherin expression at the cell-cell contacts. Conversely, loss of lateral domain is evidenced by a decrease in E-cadherin expression. In clear contrast, apical surface is clearly characterized by the expression of Podocalyxin/gp135 or Ezrin as well as Crumb/Par6/atypical PKC (22). Localization of Par complex is determined by a small GTPase, Cdc42. Other small GTPases are also participated in organizing cell polarity and changing cell shapes (22), because Rho family GTPases are well known to regulate actin cytoskeleton in the presence or absence of cell-cell contacts.

In this study, we aimed at investigating how ephrinA1/EphA2 signal induces compaction with polarization of MDCK cells. Ezrin was essential for maintaining the flat morphology of the cells. EphrinA1/EphA2 signal inactivated Rho-Rho kinase signal that phosphorylates Ezrin, thereby inducing compaction of MDCK cells.

EXPERIMENTAL PROCEDURES

Reagents, Antibodies, and siRNAs—Reagents were purchased as follows: nonclustered EphrinA1-Fc, and Control Fc from R & D Systems; Y-27632 from Calbiochem; and neomycin from Sigma-Aldrich. Anti-gp135 antibody and anti-phosphatidylinositol 4-phosphate 5-kinase antibodies were gifts from W. J. Nelson (Stanford University) and Y. Kanaho (Tsukuba University, Tsukuba, Japan), respectively. Other antibodies were purchased as follows: anti-Ezrin/Radixin/Moesin, anti-phospho-ERM detecting phosphorylation of Ezrin (Thr-567)/Radixin (Thr-564)/Moesin (Thr-558) (41A3), anti-p190RhoGAP-A, and anti-PIP5K1C from Cell Signaling Technology; anti-Ezrin (3C12), anti-EphA2 (C-20), anti-RhoA (26C4), and anti-Arf6 (3A-1) from Santa Cruz Biology; anti-E-cadherin (clone ECCD-2) from Takara Bio Inc.; anti-FLAG (M2), and anti-β-actin from Sigma-Aldrich; anti-phosphotyrosine (4G10® Platinum) from Millipore; anti-ZO-1, rhodamine-phalloidin, and Alexa Fluor 633 phalloidin from Invitrogen; anti-HA (3F10) from Roche Applied Science; horseradish peroxidase-coupled goat anti-mouse, anti-rat, and anti-rabbit IgG from GE Healthcare and Cell Signaling Technology, respectively; and Alexa Fluor 488- and Alexa Fluor 546-labeled secondary antibodies from Molecular Probes. siRNAs targeting the genes and their irrelevant siRNAs duplex were purchased from Sigma-Aldrich.

Nucleotide sequences for siRNAs used were as follows: for Ezrin number 1, 5′-GCCUUAGGGAAGUGUGGUA-3′; for Ezrin number 2, 5′-CCAAGUGAAGGAGGGAAUU-3′; for RhoA number 1, 5′-CCGGAAGAAACUGGUGAUU-3′; for RhoA number 2, 5′-GCAGGUAGAGUUGGCUUUG-3′; for Arf6, 5′-GCACCGCAUUAUCAAUGACC-3′; for p190-RhoGAP-A, 5′-GCUACUCAUAUGUACGAUA-3′; for PIP5KA number 1, 5′-GCAACUCCUGCAUUACUUA-3′; for PIP5KA number 2, 5′-CCACAGCUAUGGAAUCCAU-3′; for PIP5KC number 1, 5′-GGAAGAAUUCCUCCCUGAA-3′; and for PIP5KC number 2, 5′-CCGCCACAGACAUCUACUU-3′.

Plasmids—cDNA fragment encoding Ezrin was amplified by PCR using the Ezrin cDNA kindly provided by Sa. Tsukita (Osaka University, Japan) as a template and a primer set containing HindIII and EcoRI sites; 5′-TTAAGCTTGCCACCATGCCCAAGCCAATCAACGTCCGGGTG-3′ and 5′-AAAGAATTCCCATGGCCTCGAACTCGTCAATGCGTTG-3′. The resulting fragment was inserted into p3xFLAG-N1 vector (designated as p3xFLAG-N1-Ezrin). The plasmid expressing a mutant Ezrin (T567D) was developed by QuikChange site-directed mutagenesis kit (Stratagene) using p3xFLAG-N1-Ezrin as a template and a primer set: 5′-AAGTATAAGGACCTGCGGCAAATCAGGCAGGGCAAG-3′ and 5′-GATTTGCCGCAGGTCCTTATACTTGTCCCTGCCTTG-3′. The plasmid expressing a mutant Ezrin that cannot bind to PIP_2 (K253N,K254N,K262N,K263N, hereafter called PIP_2 mut) was developed using p3xFLAG-N1-Ezrin as a template and primer sets: 5′-TCTTTCAACGACAATAACTTTGTCATTAAGCCCATC-3′, 5′-CTTAATGACAAAGTTATTGTCGTTGAAAGAGATGTTC-3′, 5′-AAGCCCATCGACAACAATGCACCTGACTTTGTGTTCTAC-3′, and 5′-AAAGTCAGGTGCATTGTTGTCGATGGGCTTAATG-3′. The plasmid expressing Ezrin resistant to siRNA for WT Ezrin, the target of siRNA was mutated using the following primer set: 5′-GGTCTCCGCGAGGTCTGGTACTTCGGCCTC-3′ and 5′-GTACCAGACCTCGCGGAGACCAATCGTC-3′. cDNA fragment encoding p190RhoGAP-A was amplified by PCR using the p190 RhoGAP-A cDNA provided by Kazusa DNA Research Institute as a template and a primer set containing NotI and BamHI sites: 5′-ATAGCGGCCGCAATGATGATGGCAAGAAAGCAAGATG-3′ and 5′-ATAGGATCCTCACAGCGTGTGTTCGGCTTGAAG-3′. The resulting fragment was inserted into p3xFLAG-C1 vector and designated as p3xFLAG-C1-p190RhoGAP-A. The plasmid expressing p190RhoGAP-A resistant to siRNA was constructed using the following primer

set in which the target site of siRNA for p190RhoGAP-A was mutated: 5′-TCGAGGCCACACATATGTATGACAATGCT-GCCGAGG-3′ and 5′-GCATTGTCATACATATGTGT-GGCCTCGATTATGTTC-3′.

Adenovirus and Infection—The cDNA encoding human EphA2 mutant, which lacks the cytoplasmic region (EphA2Δcyto, amino acids 1–574), was amplified by PCR using human EphA2 cDNA (a gift from A. Sakakibara, Nagoya University) as a template. The amplified fragment was subcloned into pCMV-HA vector. cDNA fragment encoding COOH-terminal HA-tagged EphA2Δcyto was inserted into the pShuttle vector (Clontech, Mountain View, CA). The adenovirus was produced by using the Adeno-X system according to the manufacturer's protocol (Clontech). Recombinant adenovirus expressing β-gal was kindly provided by M. Matsuda (Kyoto University). The subconfluent MDCK cells were infected with adenoviruses at the appropriate of multiplicity of infection for 24 h and replated for the experiments.

Cell Culture, Transfection, and siRNA-mediated Protein Knockdown—MDCK cells, obtained from S. Tsukita (Osaka University) were cultured as described previously (20). The cells were placed onto ~35- and ~100-mm plastic plates at 3×10^5 cells and cultured for 48 h to obtain confluent and sparse cell cultures, respectively. MDCK cells were transfected with cDNA or oligonucleotide duplexes by using a reverse transfection method, according to the manufacturer's instructions (Invitrogen). In brief, the cells were trypsinized, washed with PBS, suspended in DMEM with 10% fetal calf serum (HyClone Laboratories), and plated onto a plastic dash in the presence of plasmid DNA or oligonucleotide duplexes mixed with Lipofectamine 2000 (Invitrogen) in OptiMEM (Invitrogen). MDCK cells for immunofluorescence studies were cultured on the glass-bottomed dishes. The cells transfected with plasmids or siRNAs for 48 h as indicated in the figures were used for the immunoblot analyses or immunofluorescence studies. MDCK cells were stimulated with 125 ng/ml of nonclustered ephrinA1-Fc or 62.5 ng/ml of control Fc during the time points indicated in the figure without any starvation. The cells were also treated with the drugs Y-27632 (20 μM) and neomycin (500 μM) for the time indicated in the figures.

Immunoprecipitation, GST-Rhotekin Pulldown Assay, and Immunoblot Analysis—The cells were washed with PBS; lysed in ice-cold lysis buffer containing 1% Nonidet P-40, 50 mM Tris-HCl, pH 7.4, 150 mM NaCl, 5 mM EDTA, 1 mM Na_3VO_4, 1 mM DTT, 1 mM phenylmethylsulfonyl fluoride, 5 μg/ml aprotinin, 2 μg/ml leupeptin, and 3 μg/ml pepstatin A; and centrifuged at 20,000 × *g* for 5 min at 4 °C. The supernatant was used for the immunoprecipitation and immunoblot analyses. Immunoprecipitation assays were performed using antibodies coupled with biotin-conjugated $F(ab')_2$ fragments of goat anti-rabbit IgG, coupled to streptavidin-Sepharose beads, as described previously (20). RhoA activity was measured using GST-rhotekin as described previously (23). The cells were lysed in a lysis buffer containing 1% Triton X-100, 20 mM Tris-HCl, pH 7.4, 100 mM NaCl, 10 mM $MgCl_2$, 1 mM EGTA, and 1 mM DTT and centrifuged at 20,000 × *g* for 10 min. The supernatant was incubated with GST-rhotekin conjugated to glutathione-Sepharose beads for 40 min at 4 °C. To enhance the detection sensitivity for RhoA on the immunoblot membrane, Can Get Signal (TOYOBO) was used to dilute the anti-RhoA antibody for immunoblot analyses.

Fractionation of Ezrin—Fractionation of soluble or insoluble Ezrin were performed as described previously (24). MDCK cells cultured on a 35-mm dish were washed twice with ice-cold PBS and scraped off in 500 μl of an ice-cold sonication buffer (150 mM NaCl, 1 mM EGTA, 1 mM DTT, 10 μg/ml leupeptin, 10 mM Hepes buffer, pH 7.5, and 20 mM NaF). The resuspended cells were sonicated in a 1.5-ml tube and centrifuged at 10,000 × *g* for 10 min at 4 °C. The supernatant and the pellet were used as soluble and insoluble fraction, respectively.

Immunofluorescence Microcopy—MDCK cells grown on the glass-bottomed dishes after the stimulation with ephrinA1-Fc or after the treatment with drugs or siRNAs were fixed in PBS containing 4% formaldehyde for 20 min at room temperature, permeabilized with 0.05% Triton X-100 in PBS for 5 min, and blocked with PBS containing 2% BSA for 10 min. The cells were incubated with first antibody for 1 h at room temperature and with Alexa 488- or Alexa 546-labeled secondary antibodies for 30 min at room temperature. To visualize F-actin, the cells were incubated with rhodamine-phalloidin or Alexa Fluor 633 phalloidin for 30 min at room temperature. Fluorescence images of Alexa Fluor 488, Alexa Fluor 546, Alexa Fluor 633, and rhodamine were recorded with a FV1000 confocal microscope (Olympus Corporation). Cell areas obtained from the XY image immunostained with anti-E-cadherin antibody were quantitatively analyzed using the MetaMorph software (Molecular Devices). The XY image shown in the figures represents a typical image obtained from at least three independent experiments. The cell area determined by the confocal XY plane of the cells was calculated using the MetaMorph software (Molecular Devices). In each image, at least more than 100 cells were used for measuring the area. The results of the quantitative analyses were shown as averages with standard deviations. Each figure of microscopical analysis shows representative results observed in at least three independent experiments.

Statistical Analysis—The values are expressed as the means ± S.D. Differences among multiple groups were compared by one-way analysis of variance followed by a post hoc comparison test with Scheffe's method or by unpaired *t* test. A p value < 0.05 was considered statistically significant.

RESULTS

Active Ezrin Maintains Flat Cell Shape and Inhibits Compaction Induced by ephrinA1 in MDCK Cells—Active Ezrin induces cell flattening, whereas ephrinA1/EphA2 signal induces compaction with polarization (20, 25). Therefore, we hypothesized that ephrinA1/EphA2 signal might affect the regulation of Ezrin. Before testing this hypothesis, we examined the expression of ERM proteins in MDCK cells and the localization of Ezrin with actin (Fig. 1*A*), because active Ezrin is known to bind actin filament. Ezrin clearly localized to the apical cell surface with actin filaments in unstimulated MDCK cells. Depletion of Ezrin by siRNAs paralleled the decrease of ERM detected by anti-ERM antibody, which recognizes all ERM family members, indicating that MDCK cells express mainly Ezrin of ERM family proteins (Fig. 1*B*).

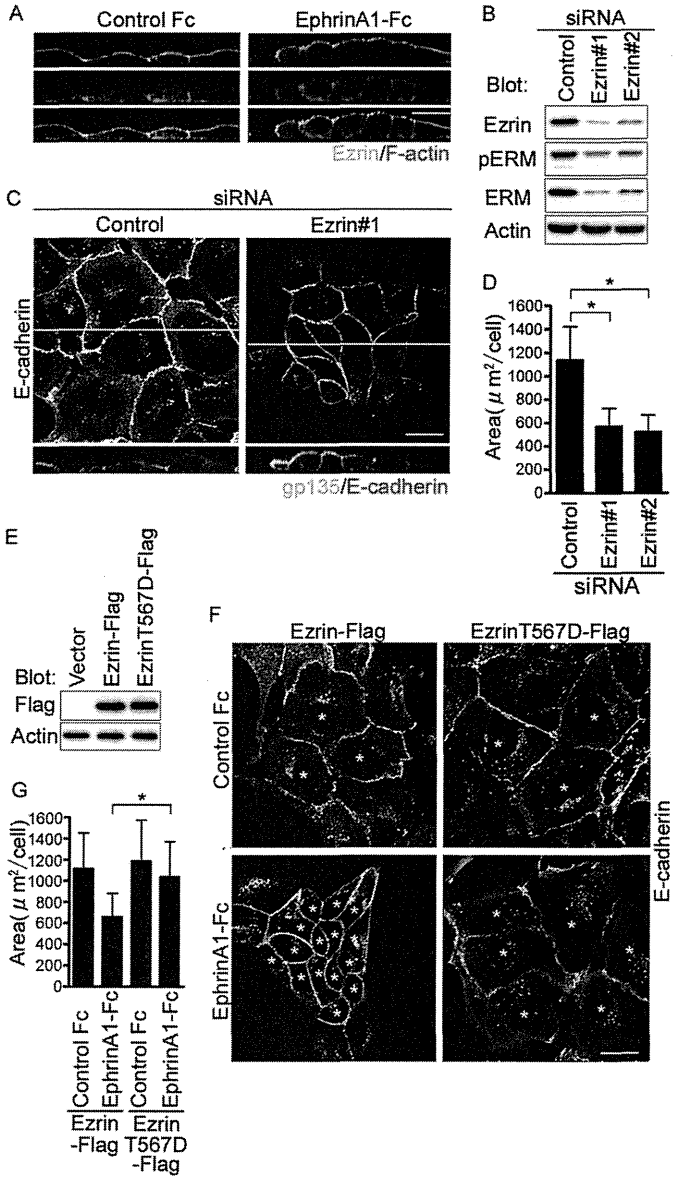

FIGURE 1. **EphrinA1/EphA2 signal induces compaction by inhibiting Ezrin that maintains the flat shape of MDCK cells.** *A*, the confocal XZ images of the MDCK cells immunostained with anti-Ezrin and stained with rhodamine-phalloidin after the stimulation of either control Fc (*left panel*) or ephrinA1-Fc (*right panel*) for 4 h. *B*, immunoblot analyses with the antibodies indicated at the *left* using the cell lysates from the MDCK cells treated with siRNAs indicated on the *top*. *C*, MDCK cells immunostained with anti-E-cadherin and anti-gp135 after the treatment with siRNAs indicated on the *top*. The confocal XY image displays the channel of Alexa 546 detecting anti-E-cadherin (*top panel*). The XZ image displays both channel of Alexa 488 detecting anti-gp135 and Alexa 546 detecting anti-E-cadherin (*bottom panel*). The *yellow line* in the XY image denotes the plane for the XZ image. *D*, area of the cells treated with siRNAs indicated at the *bottom* in *E* was calculated by measuring the individual cell area (at least more than 100 cells in each experiment) using the MetaMorph as described under "Experimental Procedures." The value (area) indicates the mean with S.D. *E*, immunoblot analyses with the antibodies indicated at the *left* using the lysates from the cells transfected with the plasmid indicated at the *top*. *F*, the confocal XY images of the cells transfected with the plasmids indicated at the *top*, stimulated with either control Fc or ephrinA1-Fc for 4 h, and immunostained with E-cadherin. *Asterisks* indicate the cells expressing Ezrin-FLAG. *G*, area of the cells marked by *asterisks* in *F* was calculated as described for *D*. *Bar*, 20 μm (throughout the figures).

To understand the loss of function of Ezrin, we imaged the MDCK cells depleted of Ezrin. Ezrin depletion resulted in compaction with polarization as evidenced by the increased height of lateral cell-cell contacts marked by E-cadherin, by the increased expression of gp135 on the apical cell surface, and by the decreased area of XY plane of individual cell (Fig. 1, *C* and *D*). We confirmed that the effect of Ezrin depletion using siRNAs on cell morphological change was indeed ascribed to the depletion of Ezrin by performing rescue experiments in which we overexpressed Ezrin resistant to the siRNA for endogenous Ezrin. When Ezrin resistant to siRNA was introduced into Ezrin siRNA-treated cells, the compaction by depletion of Ezrin was reversed (supplemental Fig. S1). Thus, these results support the notion that Ezrin is essential for the maintenance of the flat cell shape of MDCK cells.

To understand the gain of function of Ezrin, we observed the MDCK cells expressing active form of Ezrin (T567D). There was no morphological change between the cells expressing WT Ezrin and those expressing active Ezrin in resting state (Fig. 1, *E–G*), suggesting that Ezrin in MDCK cells is active without any stimulation. We further investigated the morphological change induced by ephrinA1 stimulation. Although MDCK cells expressing WT Ezrin exhibited compaction, those expressing Ezrin T567D resistant to dephosphorylation kept their flat cell shape (Fig. 1*F*). These data suggest that Ezrin functions to maintain the flat shape and might be inactivated by ephrinA1 stimulation.

Negative Regulation of Ezrin by ephrinA1/EphA2 Signal—To examine whether the activity of Ezrin is regulated by ephrinA1-triggered signaling, we investigated the phosphorylation of Ezrin that reflects its activity (Fig. 2*A*). When MDCK cells were stimulated with ephrinA1, Ezrin among ERM proteins were dephosphorylated in a time-dependent manner. Consistently, the cells stimulated with ephrinA1 became compact in parallel with dephosphorylation of Ezrin (Fig. 2*B*). EphA2 is known to be activated in epithelial cells cultured at confluent condition (20, 26). We examined the relevance of EphA2 activation to the dephosphorylation of Ezrin (Fig. 2*C*). Presumably, EphA2 was activated by ephrinA ligand expressed on MDCK cells. Dephosphorylation of Ezrin correlated with the activation of EphA2. This result was consistent with the result obtained in the MDCK cells stimulated with ephrinA1-Fc.

We further confirmed the essential signal mediated by ephrinA1-EphA2 by overexpressing EphA2 lacking the cytoplasmic domain (EphA2Δcyto) that could sequester ephrinA1 or other EphA ligands, because we could not completely exclude the involvement of EphA family receptors besides EphA2 upon ephrinA1 stimulation. Overexpression of EphA2Δcyto resulted in the reduced phosphorylation of EphA2 by ephrinA1 (Fig. 2*D*). We confirmed that most of the cells expressed the mutant EphA2 when the cells were adenovirally infected (supplemental Fig. S2). Conversely, dephosphorylation upon ephrinA1 stimulation was reversed. Consistently, the columnar shape change promoted by ephrinA1 stimulation was abrogated in the cells expressing this mutant EphA2 (Fig. 2, *E* and *F*), indicating the essential role for EphA2 in ephrinA1-triggered signal and ephrinA1-induced dephosphorylation of Ezrin.

Although Ezrin was dephosphorylated by ephrinA1 stimulation, the localization of Ezrin on the apical surface of MDCK cells was not changed. However, it was of note that phosphorylated Ezrin on the apical domain was clearly decreased after

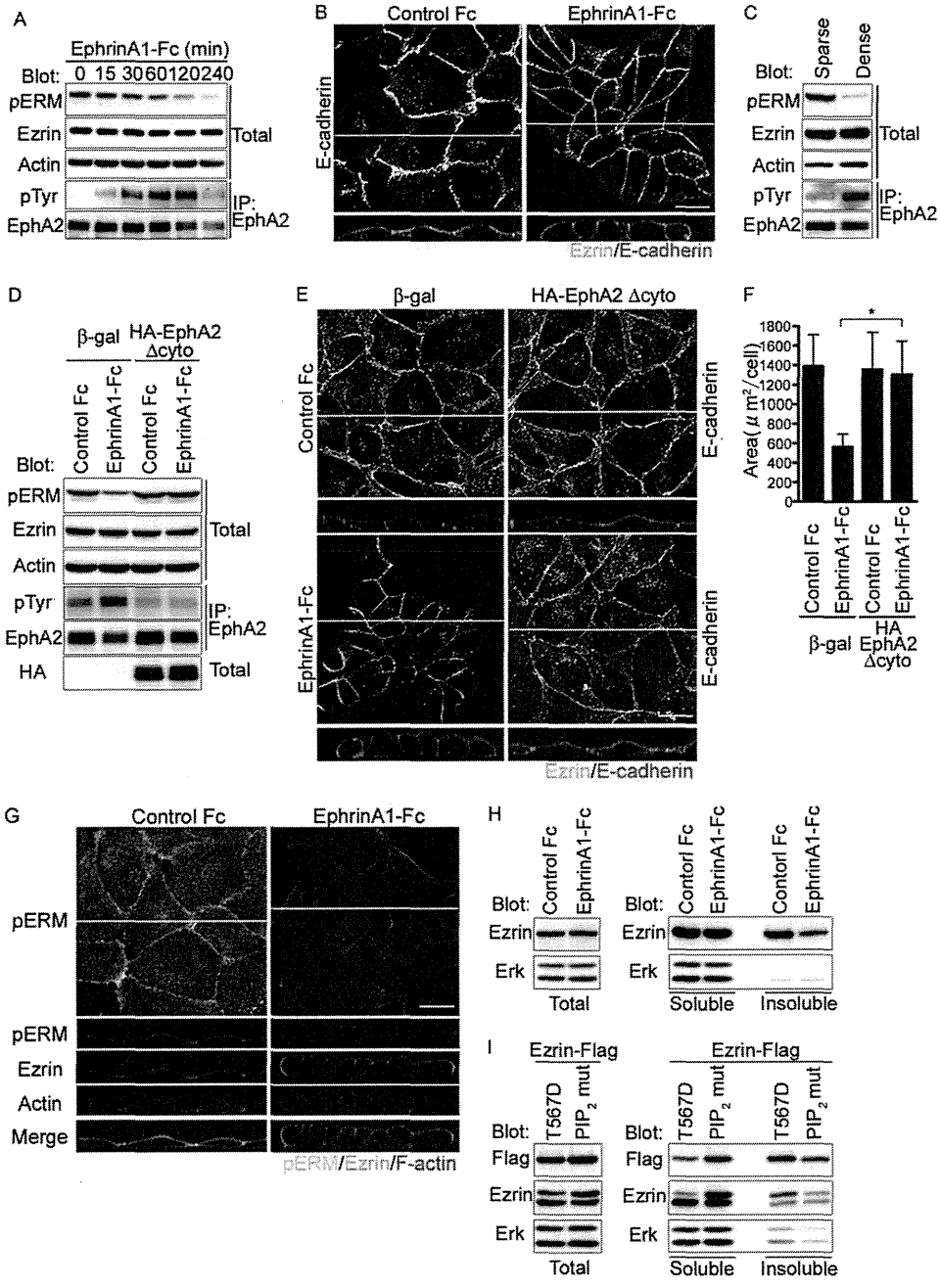

FIGURE 2. **EphrinA1/EphA2 signal induces dephosphorylation of Ezrin.** *A*, immunoblot analyses using the antibodies indicated at the *left* using the cell lysates (total) or the immunoprecipitates with anti-EphA2 (*IP: EphA2*) prepared from the cells treated with ephrinA1-Fc during the time indicated at the *top*. *B*, the confocal images of MDCK cells immunostained with anti-Ezrin and anti-E-cadherin after the stimulation with either control Fc (*left*) or ephrinA1-Fc (*right*) for 4 h. The XY image displays the channel of Alexa 546 detecting anti-E-cadherin. The XZ image displays two channels of both Alexa 488 detecting anti-Ezrin and Alexa 546 detecting anti-E-cadherin. The *yellow line* denotes the plane for the confocal XZ image. *C*, immunoblot analyses with the antibodies indicated at the *left* using the cell lysates (total) or the immunoprecipitates with anti-EphA2 (*IP: EphA2*) from the cells cultured at either sparse or dense condition. *D*, immunoblot analyses of the immunoprecipitates using anti-EphA2 (*IP: EphA2*) or cell lysate (total) from the MDCK cells infected with the adenovirus expressing either β-galactosidase (*β-gal*) or HA-tagged EphA2 lacking cytoplasmic domain (HA-EphA2Δcyto) indicated at the *top* using antibodies indicated at the *left*. *E*, confocal images of the MDCK cells infected with the adenovirus indicated at the *top* after the treatment of either control Fc (*upper panels*) or ephrinA1-Fc (*lower panels*). The *top* (XY) and *bottom* (XZ) *panels* were the confocal images for the cells immunostained with anti-E-cadherin or with both anti-E-cadherin and anti-Ezrin, respectively. The *yellow lines* in the XY image denote the plane for the confocal XZ image. *F*, quantitative analyses of the individual cell area calculated using XY images of *E*. *G*, the image for phospho-ERM (*top panels*) is the projection image of stacked XY image. The *lower panels* are the confocal images of the MDCK cells immunostained with anti-phospho-ERM (*pERM*) or anti-Ezrin and stained with Alexa Fluor 633 phalloidin after ephrinA1-Fc stimulation. The XZ images display the merged image of pERM, Ezrin, and F-actin (*bottom panel*). *H*, immunoblot analyses of the lysate (*left panel*) and the soluble or insoluble fraction (*right panel*) of the MDCK cells treated with either ephrinA1-Fc using the antibodies indicated at the *left*. *I*, immunoblot analyses of MDCK cells fractioned after the transfection with the plasmids expressing FLAG-tagged either the phosphorylation mimic mutant (T567D) or that incapable of PIP_2 binding (PIP_2 mut) as described under "Experimental Procedures" using the antibodies indicated at *left*.

the ephrinA1 stimulation (Fig. 2, *B* and *G*). We assumed that the columnar shape changes of the MDCK cells induced by ephrinA1 stimulation must be accompanied with actin cytoskeletal change. Because phosphorylated Ezrin on Thr-567 is thought to bind to actin, we quantitatively analyzed the amount of Ezrin binding to actin before and after ephrinA1 stimulation.

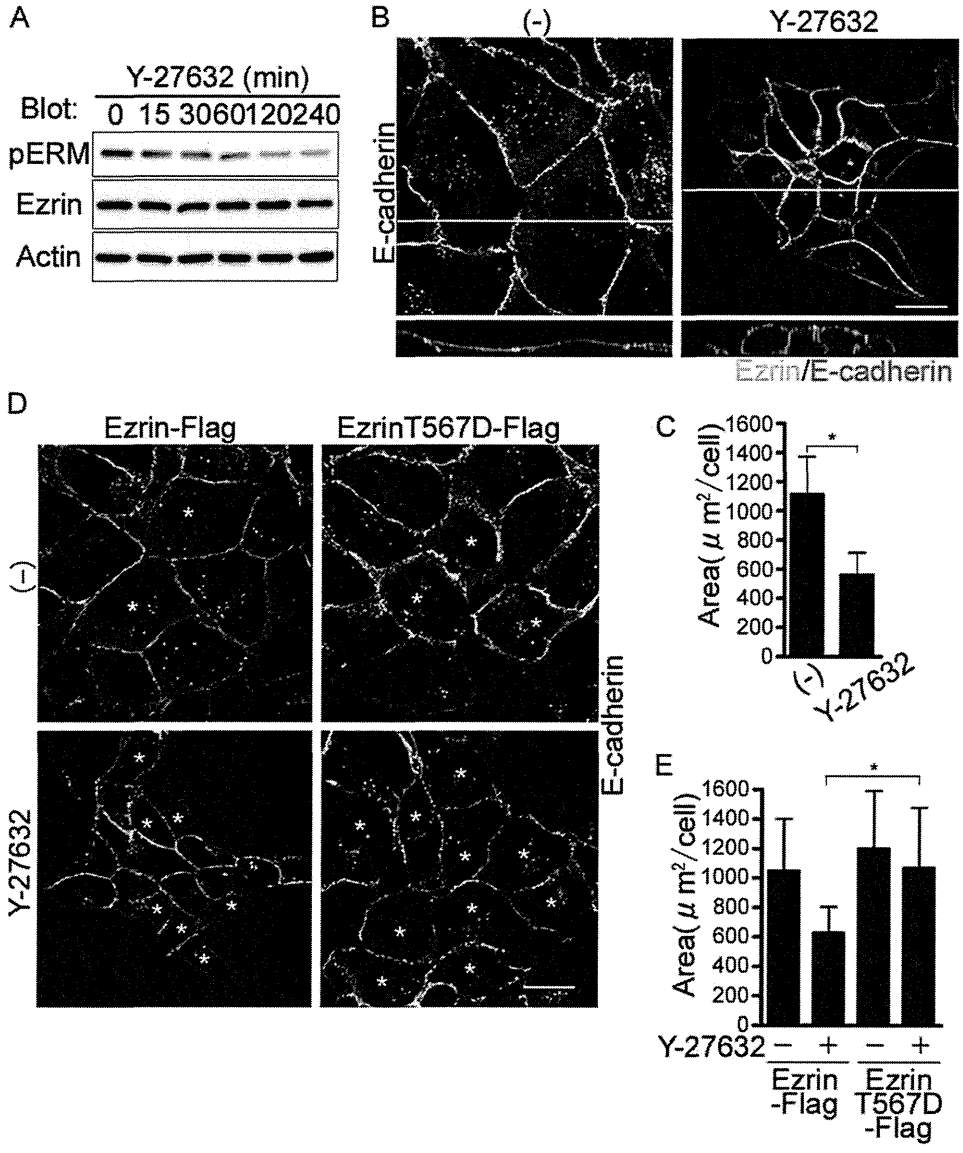

FIGURE 3. **Inhibition Rho kinase leads to the dephosphorylation of Ezrin and compaction of MDCK cells.** *A*, immunoblot analyses with the antibodies indicated at *left* using the cell lysates from the MDCK cells treated with a Rho kinase inhibitor, Y-27632, for the time indicated at the *top*. *B*, the confocal images of the cells treated with Y-27632 for 4 h were obtained as described in the legend of Fig. 2*B*. *C*, area of the XY plane was analyzed as described in the legend of Fig. 1*D*. *D*, confocal images of the MDCK cells transfected the plasmids indicated at the *top* and treated with either vehicle (−) or a Rho kinase inhibitor, Y-27632, and immunostained with anti-E-cadherin. *Asterisks* denote the cells expressing Ezrin-FLAG or EzrinT567D-FLAG. *E*, quantitative analyses of the cell area calculated using the XY images in *D*.

Ezrin bound to actin filaments detected in insoluble fraction was decreased in the MDCK cells stimulated with ephrinA1 (Fig. 2*H*). The correct fractionation was confirmed by the data that T567D mutant was increased in insoluble fraction, whereas a mutant Ezrin incapable of binding to PIP_2 was increased in soluble fraction (Fig. 2*I*). Collectively, these results suggest that the ephrinA1/EphA2 signal negatively regulates Ezrin by promoting dephosphorylation of Ezrin at the apical surface of MDCK cells and induces dissociation of actin filaments from Ezrin for the morphological changes.

RhoA-Rho Kinase Signal Is Required for Maintaining Flat Cell Shape—To understand how Ezrin is phosphorylated in the resting MDCK cells, we first examined the effect of Rho kinase inhibitor Y-27632 on phosphorylation of Ezrin, because phosphorylation of Thr-567 is known to be regulated by Rho kinase (13). Phosphorylation of Ezrin decreased in a time-dependent manner (Fig. 3*A*). MDCK cells treated with Y-27632 became compact as those depleted of Ezrin did (Figs. 3, B and *C*, and 1, *C* and *D*). The columnar cell change with increased lateral domain marked by E-cadherin was observed in the three-dimensional confocal image as in those depleted of Ezrin (Fig. 3, *B* and *C*). The cell compaction was also evidenced by the decrease in the area of XY image of individual cell (Fig. 3*C*). In contrast, the MDCK cells expressing a mutant Ezrin that mimicked the constitutive phosphorylation of Thr-567 (T567D) did not change cell shape (Fig. 3, *D* and *E*). These data suggest that the phosphorylation of Ezrin by Rho kinase is essential for maintaining flat cell shape in MDCK cells.

We then tried to test whether RhoA is responsible for Rho kinase-dependent phosphorylation of Ezrin. Depletion of RhoA using RhoA siRNAs led to the dephosphorylation of Ezrin (Fig. 4*A*). Consistently, RhoA-depleted cells showed columnar shape

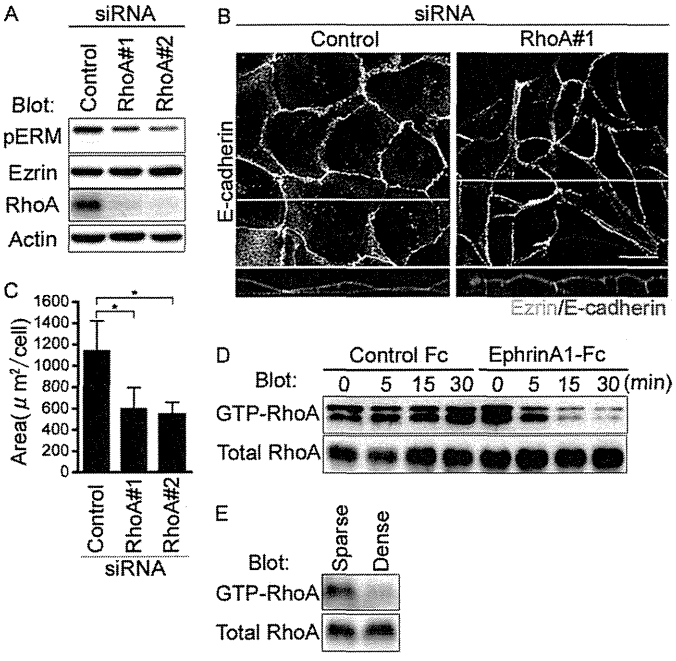

FIGURE 4. **EphrinA1/EphA2 signal inactivates RhoA that is required for maintaining the flat shape of MDCK cells.** *A*, immunoblot analyses with the antibodies indicated at the *left* using the cell lysates of the MDCK cells treated with siRNAs indicated at the *top*. *B*, the confocal images of the cells transfected with siRNAs indicated at the *top* were obtained as described in the legend of Fig. 2*B*. *C*, area was calculated as described in the legend of Fig. 1*D*. *D* and *E*, pulldown analyses with the antibodies indicated at the *left* using the lysates of the MDCK cells stimulated with ephrinA1-Fc (*D*) or those cultured at different density (*E*).

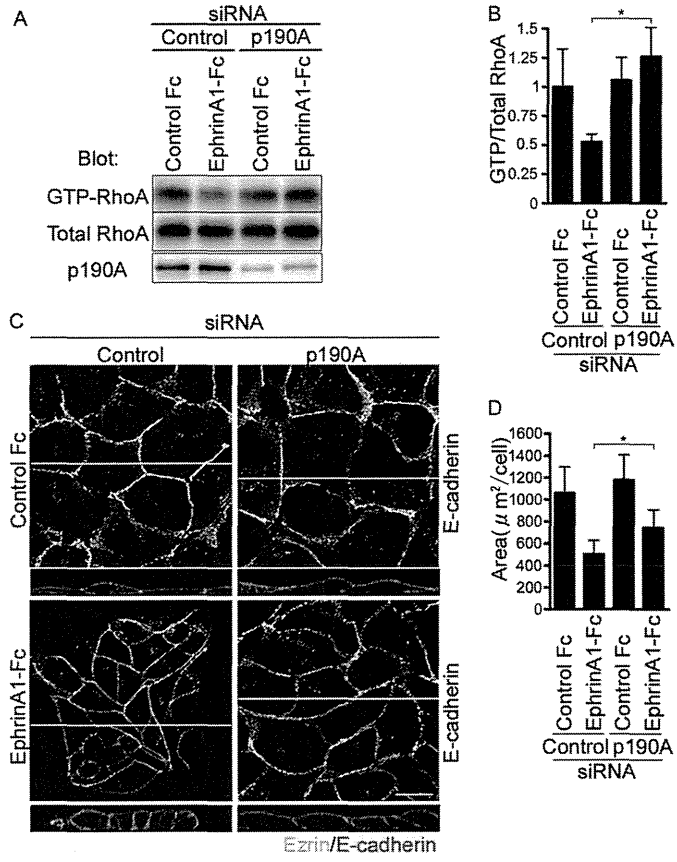

FIGURE 5. **EphrinA1/EphA2 signal induces cell compaction in a manner dependent on p190RhoGAP-A.** *A*, pulldown analyses of GTP-bound RhoA using the lysates from the cells depleted of p190RhoGAP-A (*p190A*) after the stimulation with ephrinA-Fc for 30 min. *B*, the result of *A* was quantitatively analyzed by calculating the intensity of the band of GTP-bound RhoA divided by that of total RhoA. *C*, the confocal images of the MDCK cells transfected with the siRNAs indicated at the *top* after the stimulation with either control Fc or ephrinA1-Fc for 4 h were obtained as described in the legend of Fig. 2*B*. *D*, area was calculated as described in the legend of Fig. 1*D*.

as those treated with Y-27632 did (Fig. 4*B*). The increased height of lateral domain indicated by the increased accumulation of E-cadherin at the cell-cell contacts shown in the XZ image was clearer in the cells depleted of RhoA than those treated with control siRNA (Fig. 4, *B* and *C*). These results indicate that activation of RhoA-Rho kinase signal is essential for phosphorylation of Ezrin that maintains the flat cell shape.

EphrinA1/EphA2 Signal Induces Inactivation of RhoA—To test whether ephrinA1/EphA2 signal-induced dephosphorylation of Ezrin is dependent on inactivation of RhoA-Rho kinase signal in MDCK cells, we measured the GTP-bound RhoA in the cells stimulated with ephrinA1 by pull-down assay. GTP-bound RhoA was decreased in a time-dependent manner in response to ephrinA1 stimulation (Fig. 4*D*). When EphA2 was activated in MDCK cells cultured at the confluent condition, Ezrin was dephosphorylated (Fig. 2*C*). Therefore, we examined whether GTP-bound RhoA is decreased under confluent condition and found that GTP-RhoA was decreased (Fig. 4*E*). These results were consistent with the previous evidence that the increased cell density parallels the decreased RhoA activation (27). These results suggest that ephrinA1/EphA2 signal inactivates Ezrin by inhibiting the RhoA-Rho kinase signal that phosphorylates Ezrin.

p190RhoGAP-A Is Essential for ephrinA1/EphA2 Signal-mediated Dephosphorylation of Ezrin and Compaction with Polarization—p190RhoGAP-A is reported to inactivate 2RhoA by accelerating hydrolysis of GTP on RhoA in MDCK cells, whereas cell-cell contacts are tightly formed (28). Thus, we hypothesized that p190RhoGAP-A might function downstream of EphA2 to inactivate RhoA upon ephrinA1 stimulation. GTP-bound RhoA was not decreased in the cells depleted of p190RhoGAP-A when stimulated with ephrinA1, whereas GTP-bound RhoA in the control cells was decreased (Fig. 5, *A* and *B*). We further studied the effect of depletion of p190RhoGAP-A on ephrinA1/EphA2 signal-induced cell compaction. There was no difference of cell shape and polarity between the control cells and those depleted of p190RhoGAP-A before the stimulation with ephrinA1. The cells treated with control siRNA exhibited columnar appearance with E-cadherin accumulation at the cell-cell contacts, whereas those depleted of p190RhoGAP-A failed to change the cell shape in response to ephrinA1 stimulation (Fig. 5, *C* and *D*).

EphrinA1-induced dephosphorylation of Ezrin was blocked in the cells depleted of p190RhoGAP-A, although phosphorylation of Ezrin was not increased (Fig. 6, *A* and *B*). Because the GAP activity of p190RhoGAP-A is increased by its tyrosine phosphorylation (29), we examined whether ephrinA1 induces the phosphorylation of p190RhoGAP-A and found that it became phosphorylated in a time-dependent manner (Fig. 6, *C* and *D*). Moreover, by overexpressing EphA2Δcyto in MDCK cells to sequester ephrinA1, we confirmed whether phosphorylation of p190RhoGAP-A was induced by ephrinA1/EphA2

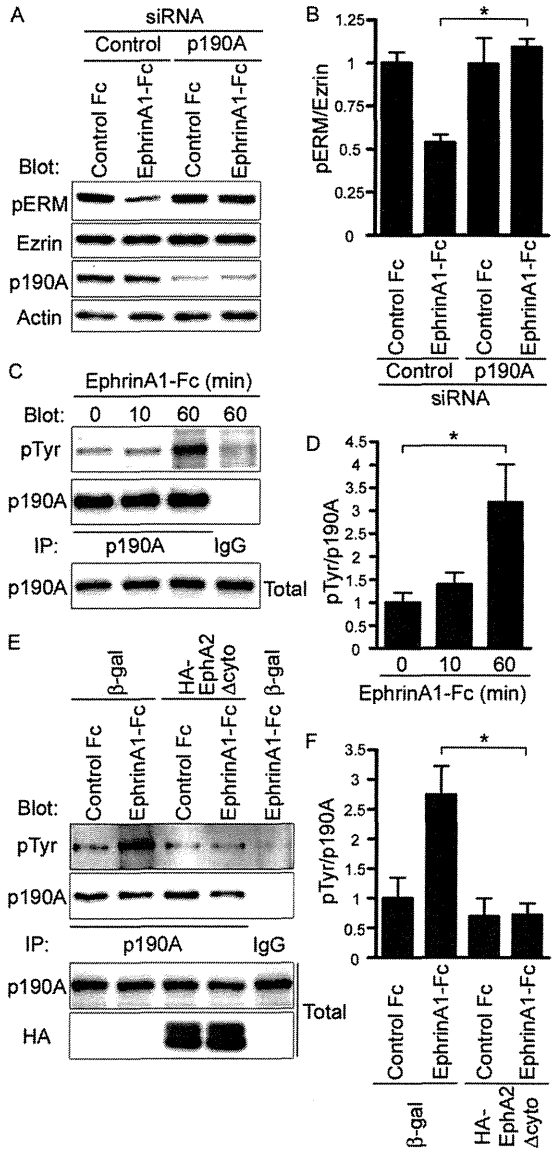

FIGURE 6. **EphrinA1/EphA2 induces phosphorylation of p190RhoGAP-A.** *A*, immunoblot analyses with the antibodies indicated at the *left* using the cell lysates prepared from the cells treated with the siRNAs before and after the stimulation with ephrinA1-Fc for 4 h. *B*, dephosphorylation of Ezrin was quantitatively analyzed by calculating the intensity of the phosphorylated Ezrin divided by that of total Ezrin using the lysates from the cells treated with siRNAs after the stimulation with ephrinA1-Fc or control as indicated at the *bottom*. *C*, immunoblot analyses with the antibodies indicated at the *left* using anti-p190RhoGAP-A immunoprecipitates (*IP*) of the MDCK cells treated with ephrinA1-Fc for the time indicated at the *top*. *D*, phosphorylation of p190RhoGAP-A quantitatively analyzed (intensity of phosopho-p190RhoGAP-A divided by that of total p190RhoGAP-A) using at least three independent immunoblots. *E*, the immunoblot analyses with the antibodies indicated at the *left* of the anti-p190RhoGAP-A immunoprecipitates (*IP*) of the cells infected with the adenovirus as described in the legend of Fig. 2*D* and treated by either control Fc or ephrinA1-Fc for 60 min. *F*, quantitative analyses of E as described in *D*.

signal. Sequestering ephrinA1 resulted in the inhibition of phosphorylation of p190RhoGAP-A (Fig. 6, *E* and *F*).

To further confirm whether p190RhoGAP-A is essential for ephrinA1-induced columnar cell change, we examined the effect of depletion of p190RhoGAP-A and that of forced expression of p190RhoGAP-A resistant to siRNA on the ephrinA1-induced cell shape change to perform a rescue experiment. The effect of depletion of p190RhoGAP-A was reversed by the mutant p190RhoGAP-A resistant to siRNA (Fig. 5*C* and supplemental Fig. S3). These data indicate that the basal RhoA activity is not regulated by p190RhoGAP-A and that ephrinA1/EphA2 signal-induced compaction is partly ascribed to the RhoA inactivation mediated by p190RhoGAP-A.

EphrinA1/EphA2 Signal Induces Dephosphorylates of Ezrin Independently of Arf6—We have previously shown that inactivation of Arf6 through the EphA2-Nck-Git1 pathway induces compaction and enhanced polarization of MDCK cells. Therefore, we determined whether Arf6 is involved in dephosphorylation of Ezrin downstream of ephrinA1/EphA2 signal. Depletion of Arf6 did not affect the dephosphorylation of Ezrin (Fig. 7*A*), although Arf6 depletion resulted in compaction of MDCK cells (Fig. 7, *B* and *C*). Therefore, we assumed the other possibility that Arf6 is involved in the activation of Ezrin, because Arf6 is implicated in the regulation of production of phosphatidylinositol via phosphatidylinositol 4-phosphate 5-kinase (PIP5K) (30). Ezrin is activated by binding to PIP_2 and being phosphorylated on Thr-567 (7, 8). Thus, we tested the effect of blocking of PIP_2 by treating the cells with neomycin that binds to PIP_2 and masks the binding site for PIP_2-binding molecules (31). Treatment of MDCK cells with neomycin reduces the phosphorylation of Ezrin and induced the compaction (Fig. 7, *D–F*), suggesting the involvement of PIP5K downstream of Arf6. We thus examined the effect of depletion of PIP5K on cell compaction. Unexpectedly, the MDCK cells treated with siRNAs for PIP5K-A and -C expressed in MDCK cells did not show any morphological changes (Fig. 7, *G–I*), excluding the possibility that PIP5K is involved in the regulation of Ezrin. These results, together with our previous data, suggest that ephrinA1/EphA2 signal induces compaction of MDCK cells by two independent mechanisms: one dependent on dephosphorylation of Ezrin and the other dependent on inactivation of Arf6 (Fig. 8).

DISCUSSION

We demonstrated that the active Ezrin (phosphorylated Ezrin on Thr-567) was essential for forming the flat shape of MDCK cells with cell-cell contacts. The importance of Ezrin in shaping the cells was evidenced by the fact that depletion of Ezrin or dephosphorylation of Ezrin resulted in the columnar cell shape change of MDCK cells. Ezrin has been reported to be involved in the determination of cell shape and polarity (7, 8). Although the active Ezrin is known to change the cell shape of MDCK cells (21, 32), the upstream signal activating Ezrin in the presence of cell-cell contacts has remained unclear. In this study, we focused on the signaling that causes dephosphorylation of Thr-567 in the MDCK cells stimulated with ephrinA1, because we previously found that ephrinA1 induces compaction of MDCK cells.

The active Ezrin inhibited the compaction, whereas depletion of Ezrin in the cells resulted in the compaction with polarity. When the active Ezrin is overexpressed in the mouse egg, the compaction that is usually found at the 8- or 16-cell stage is inhibited (33). In addition, the active Ezrin induces the formation of abnormal membrane protrusions (33). These morphological changes are also observed in MDCK cells expressing

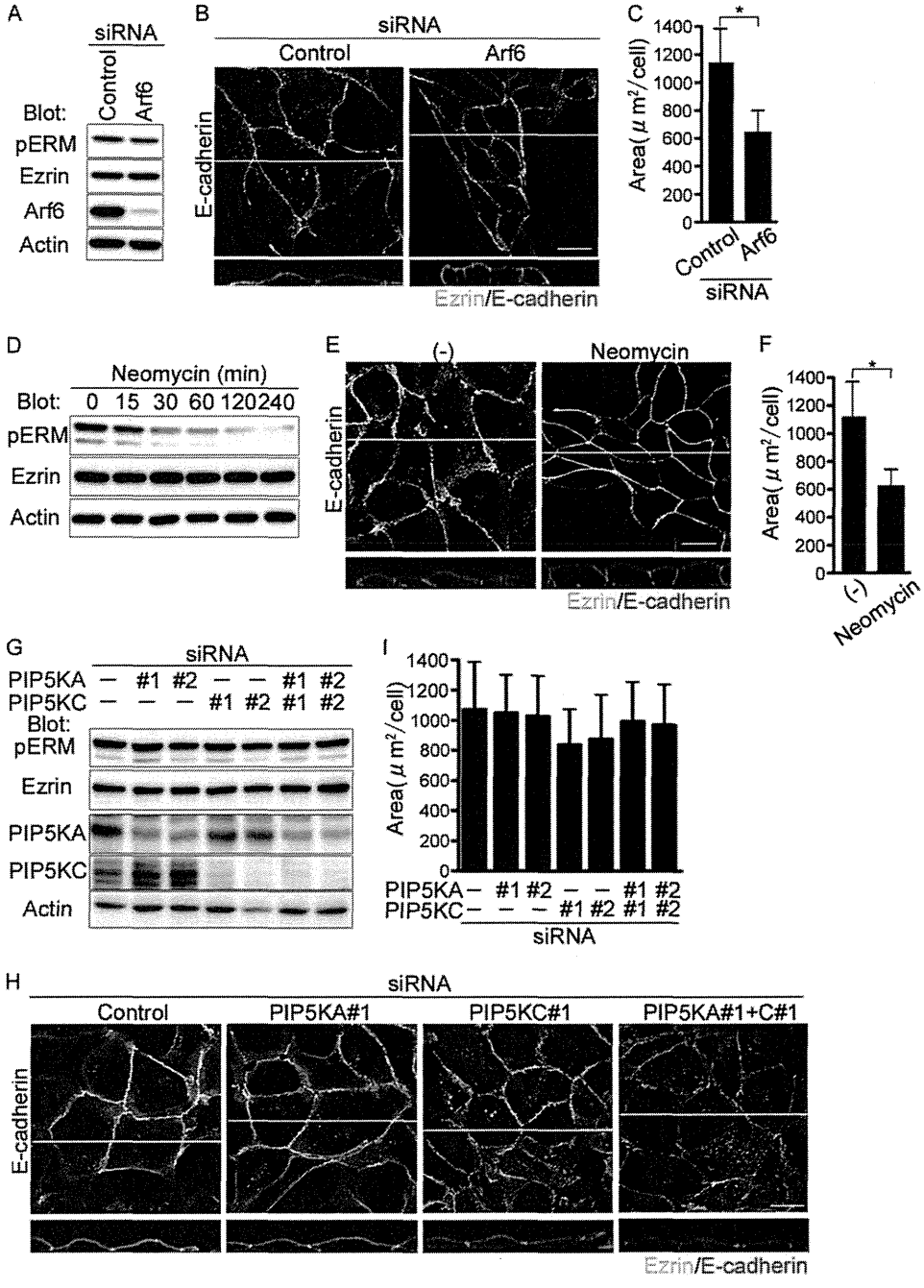

FIGURE 7. **EphrinA1/EphA2 signal induces cell compaction via inactivation of Ezrin independently of Arf6-mediated signaling.** *A*, immunoblot analyses with the antibodies indicated at the *left* using the cell lysates of the MDCK cells treated with siRNAs indicated at the *top*. *B*, the confocal images of the cells transfected with siRNAs indicated at the *top* are shown as described in the legend of Fig. 2*B*. *C*, area was analyzed as described in the legend of Fig. 1*D*. *D*, immunoblot analyses with the antibodies indicated at the *left* using the cell lysates from the MDCK cells treated with neomycin during the time indicated at the *top*. *E*, confocal images of the MDCK cells treated with neomycin for 4 h were obtained as described in the legend of Fig. 2*B*. *F*, area of the cells treated with neomycin was calculated as described in the legend of Fig. 1*D*. *G*, immunoblot analyses with the antibodies indicated at the *left* using the lysates from the MDCK cells treated with the siRNAs for PIP5K-A (*PIP5KA*) and/or PIP5K-C (*PIPK5C*). *H*, the confocal images of the cells treated with siRNAs indicated at the *top* were shown as described in the legend of Fig. 2*B*. *I*, area of the cells of *H* was quantitatively analyzed as described in the legend of Fig. 1*D*.

Ezrin T567D (32). Ezrin knock-out mice show the loss of villous morphogenesis (34), suggesting that active Ezrin might have the membrane extension activity. Consistently, we found that MDCK cells expressing active Ezrin exhibited a flat shape by horizontally extending the membrane even though cell-cell contacts were preserved.

For Ezrin, cycling between inactivation and activation might be important for shaping the cells to form the organs and tissues. In Ezrin knock-out mice, disorganized intestinal epithelial cells without polarization are found (34), suggesting the important role for Ezrin in the formation of a multicellular epithelium. Activation or inactivation of Ezrin parallels phosphorylation or dephosphorylation of Thr-567. Extracellular stimuli, including epidermal growth factor, platelet-derived growth factor, and hepatocyte growth factor, can induce the phosphorylation of Thr-567 through Ser/Thr kinases including protein

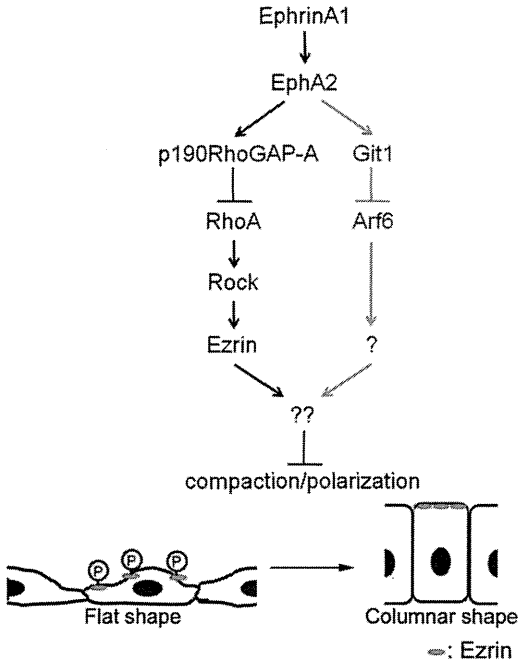

FIGURE 8. **A schematic illustration of ephrinA1/EphA2 signal-induced compaction of MDCK cells.** The signaling delineated in this study is indicated by the *black arrows* and *black characters*, whereas the previously identified signal is indicated by *gray arrows* and *gray characters*. EphrinA1/EphA2 signal induces activation of p190RhoGAP-A and subsequent inactivation of RhoA-Rho kinase that phosphorylates Ezrin. Phosphorylated Ezrin is required for maintaining the flat shape of MDCK cells. Therefore, ephrinA/EphA signal induces compaction with polarity in MDCK cells by inactivating Ezrin, although the localization of Ezrin to the apical domain is unchanged before and after ephrinA1 stimulation or upon cell-cell contact.

kinase Cα, Rho kinase, and NF-κB-inducing kinase (14, 25). Activation of Fas, T-cell receptor and B-cell receptor leads to dephosphorylates ERM protein (35–38). We here reported that ephrinA1/EphA2 induced dephosphorylation of Thr-567 via inactivation of RhoA-Rho kinase through p190RhoGAP-A. These data indicate that the formation of cell-cell contact negatively regulates Ezrin and vice versa, because Ezrin decreases the height of lateral domain at the cell-cell contacts. Therefore, activation and inactivation of Ezrin appear to be essential for organogenesis that requires the cell-cell contacts.

Besides the activation of Ezrin indicated by phosphorylation of Thr-567, PIP_2 was required for activated Ezrin-dependent morphological change (Fig. 7). It is controversial whether ephrinA/EphA signal activates phosphatidylinositol 3-kinase. EphrinA1 stimulation results in the recruitment of Src homology 2-containing inositol-5′-phosphatase and subsequently inhibiting the conversion from PIP_2 to phosphatidylinositol 3,4,5-triphosphate (39), suggesting the possibility of an increase in PIP_2. In contrast, there is a contrasting report that EphA2 activation leads to the activation of phosphatidylinositol 3-kinase in endothelial cells (40, 41), suggesting the possibility of a decrease in PIP_2. PIP5 kinase is an effector of Arf6 (30). We previously demonstrated that ephrinA1/EphA2 signal induces compaction of MDCK cells via inactivation of Arf6 and found that PIP_2 was essential for maintaining the flat morphology of MDCK cells in this study (Fig. 7). We thus tried to explore whether ephrinA1/EphA2 signal affected the localization of Ezrin in a manner dependent on PIP_2. Depletion of PIP5K did not result in any morphological changes, excluding the possibility that Arf6-PIP5K-mediated PIP_2 regulation in ephrinA1/EphA2 signal induces compaction. In addition, Arf6 depletion did not affect dephosphorylation of Ezrin (Fig. 7*A*). These results indicate that ephrinA1/EphA2 signal mainly regulates the inactivation of Ezrin by inhibiting RhoA-Rho kinase signal in a manner independent on Arf6, although it is not clear whether EphA2 phosphorylates p190RhoGAP-A directly or indirectly via other tyrosine kinases.

The changes of cell shape are accompanied with the changes in the domains of plasma membrane, pointing to the polarity. Throughout the experiments, the localization of Ezrin was restricted to the apical domain even in flat or columnar states, suggesting that the activation or inactivation is not dependent on the localization of Ezrin but dependent on the degree of phosphorylation of Thr-567. At present, we have not yet clarified the downstream signaling that controls cell morphology by Ezrin at the apical domain, although we here demonstrated the regulation of phosphorylation by ephrinA1/EphA2 signaling initiated by cell-cell contacts. Ezrin at the border between apical domain and lateral domain is known to bind to actin filament and to Bitesize to control actin organization at the cell-cell junction (42). It is required to explore the molecular mechanism by which active Ezrin maintains the flat morphology. In conclusion, we delineated the signal that regulates ephrinA1/EphA2-induced compaction of MDCK cells (Fig. 8): the engagement ephrinA1 with EphA2 results in the phosphorylation of p190RhoGAP-A and subsequent inactivation of RhoA-Rho kinase signaling, thereby leading to the dephosphorylation of Thr-567 of Ezrin that is essential for maintaining the flat morphology of MDCK cells.

Acknowledgments—We are grateful to W. J. Nelson (Stanford University) for anti-gp135 antibody, Y. Kanaho (Tsukuba University) for anti-PIP5K antibodies, S. Tsukita (Osaka University) for Ezrin cDNA, A. Sakakibara for EphA2 cDNA, S. Ohno and A. Suzuki (Yokohama City University) for helpful comments. We also thank M. Sone, K. Hiratomi, and Y. Matsuura for technical assistance.

REFERENCES

1. Takeichi, M. (1991) *Science* **251,** 1451–1455
2. Gumbiner, B. M. (2005) *Nat. Rev. Mol. Cell Biol.* **6,** 622–634
3. Kalluri, R., and Weinberg, R. A. (2009) *J. Clin. Invest.* **119,** 1420–1428
4. Thiery, J. P., Acloque, H., Huang, R. Y., and Nieto, M. A. (2009) *Cell* **139,** 871–890
5. St Johnston, D., and Ahringer, J. (2010) *Cell* **141,** 757–774
6. Adams, C. L., Chen, Y. T., Smith, S. J., and Nelson, W. J. (1998) *J. Cell Biol.* **142,** 1105–1119
7. Bretscher, A., Edwards, K., and Fehon, R. G. (2002) *Nat. Rev. Mol. Cell Biol.* **3,** 586–599
8. Fehon, R. G., McClatchey, A. I., and Bretscher, A. (2010) *Nat. Rev. Mol. Cell Biol.* **11,** 276–287
9. Tsukita, S., Oishi, K., Sato, N., Sagara, J., Kawai, A., and Tsukita, S. (1994) *J. Cell Biol.* **126,** 391–401
10. Orlando, R. A., Takeda, T., Zak, B., Schmieder, S., Benoit, V. M., McQuistan, T., Furthmayr, H., and Farquhar, M. G. (2001) *J. Am Soc. Nephrol.* **12,** 1589–1598
11. Martín-Villar, E., Scholl, F. G., Gamallo, C., Yurrita, M. M., Muñoz-Guerra, M., Cruces, J., and Quintanilla, M. (2005) *Int. J. Cancer* **113,** 899–910